



Si Isotope Variability in Proterozoic Cherts

Citation

Chakrabarti, Ramananda, Andrew Herbert Knoll, Stein B. Jacobsen, and Woodward W. Fischer. 2012. Si isotopic variability of Proterozoic cherts. *Geochimica et Cosmochimica Acta* 91:187-201.

Published Version

doi:10.1016/j.gca.2012.05.025

Permanent link

<http://nrs.harvard.edu/urn-3:HUL.InstRepos:10860682>

Terms of Use

This article was downloaded from Harvard University's DASH repository, and is made available under the terms and conditions applicable to Open Access Policy Articles, as set forth at <http://nrs.harvard.edu/urn-3:HUL.InstRepos:dash.current.terms-of-use#OAP>

Share Your Story

The Harvard community has made this article openly available.
Please share how this access benefits you. [Submit a story](#).

[Accessibility](#)

1 **Si isotope variability in Proterozoic cherts**

2
3 Ramananda Chakrabarti^{1*#}, Andrew H. Knoll^{1,2}, Stein B. Jacobsen¹, Woodward W.
4 Fischer³

5
6 1. Department of Earth and Planetary Sciences, Harvard University, Cambridge, MA
7 02138

8 2. Department of Organismic and Evolutionary Biology, Harvard University, Cambridge,
9 MA 02138

10 3. Division of Geological and Planetary Sciences, California Institute of Technology,
11 Pasadena, CA 91125

12
13
14 * Corresponding author # Present address: Center for Earth Sciences, Indian Institute of
15 Science, Bangalore, Karnataka 560 012, India (ramananda@ceas.iisc.ernet.in;
16 ramananda@gmail.com; Tel: +91-80-2293-3003)

17
18 Emails:

19 Ramananda Chakrabarti (ramananda@gmail.com; ramananda@ceas.iisc.ernet.in)

20 Andrew H. Knoll (aknoll@oeb.harvard.edu)

21 Stein B. Jacobsen (jacobsen@neodymium.harvard.edu)

22 Woodward W. Fischer (wfischer@caltech.edu)

23
24
25
26
27
28
29
30
31

32 **Abstract**

33 We report Si-isotopic compositions of 75 sedimentologically and petrographically
34 characterized chert samples with ages ranging from ~2600 to 750 Ma using multi-
35 collector inductively coupled plasma mass spectrometry. $\delta^{30}\text{Si}$ values of the cherts
36 analyzed in this study show a ~ 7‰ range, from -4.29 to +2.85. This variability can be
37 explained in part by 1) simple mixing of silica derived from continental (higher $\delta^{30}\text{Si}$)
38 and hydrothermal (lower $\delta^{30}\text{Si}$) sources, 2) multiple mechanisms of silica precipitation
39 and 3) Rayleigh-type fractionations within pore waters of individual basins.

40 We observe ~3 ‰ variation in peritidal cherts from a single Neoproterozoic
41 sedimentary basin (Spitsbergen). This variation can be explained by Rayleigh-type
42 fractionation during precipitation from silica-saturated porewaters. In some samples,
43 post-dissolution and reprecipitation of silica could have added to this effect. Our data also
44 indicate that peritidal cherts are enriched in the heavier isotopes of Si whereas basinal
45 cherts associated with banded iron formations (BIF) show lower $\delta^{30}\text{Si}$. This difference
46 could partly be due to Si being derived from hydrothermal sources in BIFs. We postulate
47 that the difference in $\delta^{30}\text{Si}$ between non-BIF and BIF cherts is inconsistent with the
48 contrasting genesis of these deposits. Low $\delta^{30}\text{Si}$ in BIF is consistent with laboratory
49 experiments showing that silica adsorbed onto Fe-hydroxide particles preferentially
50 incorporates lighter Si isotopes.

51 Despite large intrabasinal variation and environmental differences, the data show
52 a clear pattern of secular variation. Low $\delta^{30}\text{Si}$ in Archean cherts is consistent with a
53 dominantly hydrothermal source of silica to the oceans at that time. The monotonically
54 increasing $\delta^{30}\text{Si}$ from 3.8 Ga to 1.5 Ga appears to reflect a general increase in continental
55 versus hydrothermal sources of Si in seawater, as well as the preferential removal of
56 lighter Si isotopes during silica precipitation in iron-associated cherts from silica-
57 saturated seawater. The highest $\delta^{30}\text{Si}$ values are observed in 1.5 Ga peritidal cherts; in
58 part, these enriched values could reflect increasing sequestration of light silica during
59 soil-forming processes, thus, delivering relatively heavy dissolved silica to the oceans
60 from continental sources. The causes behind the reversal in trend towards lower $\delta^{30}\text{Si}$ in
61 cherts younger than 1.5 Ga old are less clear. Cherts deposited 1800-1900 Ma are

62 especially low $\delta^{30}\text{Si}$, a possible indication of transiently strong hydrothermal input at this
63 time.

64

65 1. INTRODUCTION

66

67 Cherts, deposits of amorphous silica now microcrystalline quartz, are ubiquitous
68 in the sedimentary rock record, documenting the evolution of the global silica cycle
69 through geologic time (Maliva et al., 1989; Maliva et al., 2005). The isotopic composition
70 of Si in Archean and Proterozoic cherts can provide insights into the sources and sinks of
71 marine silica before the evolution of silica-precipitating sponges, radiolarians and
72 diatoms. However, the use of sedimentary silica as a direct proxy for the composition and
73 physical state of Precambrian seawater has limitations because most Precambrian cherts
74 formed during the diagenesis of precursor sediments. Robert and Chaussidon (2006)
75 measured the Si isotopic composition of an extensive set of chert samples, primarily from
76 Archean and Proterozoic successions, but also including Phanerozoic examples, using an
77 ion-microprobe technique. They interpreted their combined O and Si isotope data from
78 Precambrian cherts to reflect seawater paleo-temperatures. Subsequent studies have
79 highlighted the importance of the source of Si in determining the isotopic composition of
80 preserved cherts (Steinboefel et al., 2009; van den Boorn et al., 2007, 2010; Heck et al.,
81 2011).

82 Improvements in mass spectrometry techniques, particularly multi-collector
83 inductively coupled plasma mass spectrometry (MC-ICPMS), now permit Si isotopes to
84 be measured with much better precision (2σ errors better than 0.1‰; e.g. Georg et al.,
85 2006b; Chakrabarti and Jacobsen, 2010). MC-ICPMS Si isotope data are also accurate to
86 better than 0.1 ‰ based on measurements of inter-laboratory standards. MC-SIMS allows
87 sampling in high resolution but is limited to a 2σ uncertainty of 0.3 ‰ for $\delta^{30}\text{Si}$ (Heck et
88 al., 2011) which, although a significant improvement compared to earlier ion-probe
89 studies (e.g. Robert and Chaussidon, 2006; Basile-Doelsch et al., 2005) is still 3 times
90 less precise than MC-ICPMS. Several recent studies have reported high-precision MC-
91 ICPMS Si isotope measurements of cherts, primarily from Archean successions
92 (Abraham et al., 2011; Andre et al., 2006; Steinboefel et al., 2009, 2010; van den Boorn

93 et al., 2007, 2010). Here we report high-precision MC-ICPMS Si isotope data for a suite
94 of well-characterized chert samples with ages ranging from ~2530 to ~750 Ma.

95 In the following sections we compare and contrast the modern and Precambrian
96 silica cycles and interpret our Si isotope measurements of Late Archean and Proterozoic
97 cherts based on the source of silica, mechanism of silica precipitation and depositional
98 setting. The data document both marked isotopic variation within individual Proterozoic
99 basins and, despite this, a clear pattern of change throughout the Proterozoic Eon, as
100 originally observed by Robert and Chaussidon (2006). Along with previously available
101 Si-isotopic measurements, our new data allow us to evaluate various mechanisms
102 proposed to explain observed temporal variations in the Si isotopic composition of
103 Precambrian cherts.

104

105 **2. SAMPLES**

106

107 We determined the Si-isotopic compositions of 75 chert samples with ages
108 ranging from ~2600 to 750 Ma (Table 1). The samples come from measured sections and
109 are well characterized sedimentologically and petrographically (see Table 1 for
110 references and Fig. 1). They include peritidal cherts, which are largely early diagenetic
111 replacements of precursor carbonate sediments, as well as basinal cherts, associated
112 primarily with iron formation, deposited in environments up to several hundred meters
113 below the sea surface. Our sample choice reflects two mutually reinforcing strategies.

114 In the first instance, given the range of $\delta^{30}\text{Si}$ values reported by Robert and
115 Chaussidon (2006), we wanted to gauge the degree of isotopic variation within a single
116 basin. Thus, we analyzed 21 samples from the ca. 800-720 Ma Akademikerbreen Group,
117 Spitsbergen, and 3 samples from its correlatives on Nordaustlandet (Knoll, 1984) and in
118 East Greenland (Green et al., 1989). This ca. 2000 m succession contains a variety of
119 shallow marine carbonate facies, including tidal flat and lagoonal carbonates, oolites, and
120 stromatolitic bioherms (Knoll and Swett, 1990). Cherts occur throughout the succession
121 as irregular to ellipsoidal nodules as well as individually silicified ooids, microbial mat
122 laminae, and thin flakes ripped up and redeposited in lagoons (Knoll et al., 1989). Field
123 and petrographic observations indicate that the silica replaced original carbonate

124 sediments early in diagenesis (Maliva et al., 1989), a conclusion corroborated by the
125 common occurrence of exceptionally well preserved microfossils in Akademikerbreen
126 cherts (Knoll, 1985; Knoll, 1984; Knoll et al., 1989; Knoll et al., 1991). Indeed, the
127 exceptional preservation of organic walled microfossils required the chert have been
128 emplaced on the timescale of organic decay, no greater than a few thousand years after
129 deposition and probably much less. Most of the cherts occur in coastal carbonates; this
130 environmental dependence is expected for early oceans without silica biomineralizing
131 protists and animals (Maliva et al., 1989). Finally, we also analyzed a pair of samples
132 from the age-equivalent Fifteenmile Group (formerly assigned to the Lower Tindir
133 Group), northwestern Canada (Allison and Awramik, 1989; Macdonald et al., 2010,
134 2011).

135 Our second strategy focused on the older end of the age spectrum. In the chert
136 dataset of Robert and Chaussidon (2006), all samples, although screened for alteration
137 using oxygen isotopes, are viewed as equivalent, in the sense that all were deemed
138 equally likely to preserve a record of seawater Si-isotopic composition. However, it is
139 clear from the sedimentary geology and petrography that these materials vary in mode of
140 formation and environmental setting, raising the question of whether long term trends
141 might principally reflect the succession in sample dominance from hydrothermal cherts in
142 the Early Archean, to iron formation in late Archean and Paleoproterozoic basins, to
143 peritidal cherts in younger Proterozoic basins (e.g. Fischer and Knoll, 2009; van den
144 Boorn et al., 2010). Added to this is the potentially complicating issue that isotope
145 fractionation accompanies silica adsorption onto iron oxides, with the lighter isotope
146 preferentially enriched in the precipitate (Delstanche et al., 2009; Opfergelt et al., 2009).
147 Thus, we analyzed 12 chert samples from the late Archean Transvaal Supergroup, South
148 Africa (Knoll and Beukes, 2009), a collection that includes peritidal cherts in carbonates,
149 deep water chert nodules and basinal iron formation. This allows us to ask whether the
150 basinal sedimentation of silica adsorbed onto iron ferrihydroxides (e.g., Fischer and
151 Knoll, 2009) imparts a detectable environmental variation onto cherts from this basin.
152 Building on this, we also analyzed a pair of samples from the Late Archean Hamersley
153 Supergroup, Australia (Yi-Liang et al., 2011), and eight samples from several 1800-1990

154 Ma successions that include late Paleoproterozoic iron formation (Barghoorn and Tyler,
155 1965; Tobin, 1990; Brotton et al., 2007; Wilson et al., 2010 and references therein).

156 Finally, to connect our Paleo- and Neoproterozoic sample sets, we analyzed silica
157 nodules in peritidal carbonates from the ca. 1000-1100 Ma Sukhaya Tunguska Formation,
158 northwestern Siberia (Sergeev et al., 1997, and references therein), the ca. 1200 Ma
159 Narssarssuk Formation, northwestern Greenland, and correlative beds of the Society
160 Cliffs, Formation, Baffin Island (Dawes, 1997; Kah and Knoll, 1996; Strother et al.,
161 1983) and the 1400-1500 Ma Billyakh Group, northern Siberia (Sergeev et al., 1995).
162 Petrographic similarities among all younger Proterozoic samples and their common
163 preservation of microfossils suggest that all of these samples are similar in depositional
164 setting, timing of formation, and mode of emplacement.

165 In addition to the above-mentioned chert samples, three inter-laboratory Si
166 isotope ratio standards IRMM-018, Diatomite, and Big Batch (Reynolds et al., 2007), two
167 in-house pure silicon standards from Alfa Aesar (Harvard-AA-Si) and High Purity
168 Standards (Harvard-HPS-Si) as well as terrestrial mantle-derived igneous rocks from
169 different tectonic settings including USGS standards BCR-1 (Columbia River basalt,
170 Bridal Veil Flow Quarry) and BHVO-1 (basalt from Halemaumau, Hawaii) were also
171 analyzed during this study. The results for the standards and silicate igneous rocks and
172 minerals have been reported elsewhere (Chakrabarti and Jacobsen, 2010).

173

174 **3. ANALYTICAL METHODS**

175

176 Hand specimen-sized samples (~ 2 cubic inch) were coarsely crushed using a rock
177 hammer. After crushing, rock chips were visually inspected for surface alteration and
178 stains. Centimeter-size rock chips were cleaned with water in an ultrasonic bath, air-dried
179 and subsequently crushed using an alumina mortar and pestle. Relatively large quantities
180 of rock chips (~0.5-1 gm) were crushed to powder to obtain a homogeneous
181 representation of each sample. For isotopic analysis, ~5 mg of rock powder was
182 dissolved.

183 For this study, a HF acid-free dissolution technique was used, similar to published
184 techniques (Georg et al., 2006b; van den Boorn et al., 2006; Chakrabarti and Jacobsen,

185 2010). About 5 mg of powdered sample was mixed with 150-200 mg of ultra-pure solid
186 sodium hydroxide (NaOH) and 50 μ l of 18 M Ω water in 5 ml in-house made Teflon
187 containers which were tightly placed in custom-made stainless steel jackets and heated to
188 \sim 200 $^{\circ}$ C in an oven for 72 hours. After dissolution, samples were transferred in \sim 100 ml
189 of 0.05N HNO $_3$. Si was separated by ion-exchange chromatography using 2ml of the
190 Bio-Rad 50W-x12 (200-400 mesh, H $^+$ form) cation exchange resin (Georg et al., 2006b).
191 Si was eluted with 4-6 ml water and the Si yield was $>$ 99% for all samples.

192 Si isotopes (masses 28, 29 and 30) were analyzed using a GV IsoProbe-P Multi-
193 Collector Inductively Coupled Plasma Mass Spectrometer (MC-ICPMS) at Harvard
194 University in high resolution mode with a resolving power ($R_{\text{power, 5\%-95\%}}$) (Weyer and
195 Schwieters, 2003) of 5000 and using an optimized proportion of H $_2$, He and Ar in the
196 collision cell of the IsoProbe-P as described previously in Chakrabarti and Jacobsen
197 (2010). We were able to resolve the $^{14}\text{N}_2\text{H}^+$ and $^{14}\text{N}^{16}\text{O}^+$ interferences on masses 29 and
198 30, respectively, and did not observe any interference on mass 28. All our samples and
199 standards lie on a mass-dependent fractionation line which indicates that using high-
200 resolution slits and collision cell gases, we were able to resolve all the potential isobaric
201 interferences on the three isotopes of Si (see Chakrabarti and Jacobsen, 2010 for details).
202 A sample-standard bracketing technique using NBS28 as the standard was used to correct
203 for instrumental mass fractionation. NBS28, a pure quartz sand, was also dissolved and
204 processed through chemistry in the same way as the samples. For all samples and the
205 bracketing standard, we ran 5 ppm solutions which resulted in a \sim 4 volt signal on mass
206 28. Si concentration of the bracketing standard and sample was matched to within 10%.
207 Total Si blanks in 1% v/v nitric acid was less than 1 mv. Hence, blank correction was not
208 necessary.

209 Sample and standard solutions were introduced into the plasma using a spray
210 chamber with heating and cooling options (APEX-IR, from Elemental Scientific Inc.)
211 attached with a self-aspirating Teflon nebulizer (ESI) with an uptake rate of 100 μ l/
212 minute. Si isotope ratio measurements were done in static mode involving a defocused (\pm
213 0.5 mass) baseline measurement at the beginning of each analysis. Data were collected in
214 one block of 25 cycles, each with an integration time of 10 seconds per cycle. Data
215 reduction was performed off-line. Delta values were determined as $\delta^{xx}\text{Si}$ (‰) =

216 $[(^{xx}\text{Si}/^{28}\text{Si})_{\text{sample}} / (^{xx}\text{Si}/^{28}\text{Si})_{\text{NBS28}} - 1] \times 1000$ where xx is either mass 29 or 30. Long-term
217 external reproducibility of our measurements is based on repeated measurements of Si
218 standards over 2 years and is better than 0.05 ‰ ($2\sigma_m$, standard error of the mean) for
219 $\delta^{30}\text{Si}$ (Chakrabarti and Jacobsen, 2010).

220

221 4. RESULTS

222

223 Our Si isotopic data for the chert samples are listed in Table 1. External
224 reproducibility is reported as $2\sigma_m$. Results of our long term measurements of the inter-
225 laboratory standards (Diatomite, IRMM-018 and Big Batch) obtained during the course
226 of this study have been published elsewhere (Chakrabarti and Jacobsen, 2010) and agree
227 with recommended values (Reynolds et al., 2007). All the above standards were
228 processed in the same way as the samples, using ion-exchange chromatography. During
229 the course of this study, we also analyzed two in-house pure silicon standards
230 (Chakrabarti and Jacobsen, 2010) from Alfa Aesar (Harvard-AA-Si) and High Purity
231 Solutions (Harvard-HPS-Si) with wide-ranging $\delta^{30}\text{Si}$ of -12.62 ± 0.02 and -0.81 ± 0.03 ,
232 respectively (Chakrabarti and Jacobsen, 2010). Si isotopic compositions of the
233 chemically purified aliquots of these pure Si standards are indistinguishable from those of
234 the unprocessed pure Si solutions, validating the accuracy of our measurements for
235 samples processed through chemical separation.

236 The $\delta^{30}\text{Si}$ values of the cherts analyzed in this study show a $\sim 7\%$ range, from
237 -4.29 to $+2.85$. Three principal patterns require explanation. First, the samples show
238 substantial variation (3-4‰) within both individual basins and time intervals. Second,
239 despite this variation, there is a distinct pattern of secular change in Si-isotope ratios,
240 from low $\delta^{30}\text{Si}$ values in early Archean (data from literature), which increases to a
241 maximum (up to 2.85) in mid-Proterozoic cherts, after which $\delta^{30}\text{Si}$ values decline toward
242 the present (Figure 2, the inferred average trend during the Precambrian is shown
243 schematically as a yellow band). Against this backdrop, values for successions that
244 contain iron formation stand out for their relatively low $\delta^{30}\text{Si}$ values ($+0.57$ to -4.29),
245 particularly those from ca. 1.8-1.9 Ga ($\delta^{30}\text{Si} = -1.57$ to -4.29), with extremely low values
246 in two samples from the Frere and Duck Creek formations.

247

248 **5. DISCUSSION**

249

250 **5.1. Si cycling and Si isotopes in the modern Earth system**

251 Continental weathering is the dominant source of silicic acid to the modern
252 oceans, delivered primarily as dissolved load in river waters (Treguer et al., 1995) (Table
253 2) as well as groundwater fluxes (Georg et al., 2009). Although the flux of suspended
254 silica-rich particles in rivers is greater than the dissolved silicic acid (H_4SiO_4) flux,
255 further dissolution of this particulate matter is slow and its contribution to the silicic acid
256 flux to the oceans is negligible (Treguer et al., 1995). Other silica sources include
257 hydrothermal fluids and seafloor weathering of basalts. Biogenic uptake of dissolved
258 silica constitutes the major sink for silicic acid in the modern oceans and the estimated
259 output balances the input (Table 2). Silica is undersaturated in modern oceans, with an
260 average concentration of H_4SiO_4 at $\sim 70 \mu\text{M}$ (2 ppm) (Treguer et al., 1995). However,
261 silica concentrations show strong lateral and vertical heterogeneity in ocean basins
262 depending on nutrient availability and uptake by diatoms in surface waters and skeleton
263 dissolution at depth (Reynolds et al., 2006). The residence time of Si in the global oceans
264 is $\sim 15,000$ years (Table 2) although, relative to biological uptake from surface waters, it
265 is only ~ 400 years (Treguer et al., 1995), implying that Si delivered to the modern oceans
266 is recycled ~ 40 times through the biological cycle before it departs into a sedimentary
267 sink.

268 Bulk igneous rocks as well as co-existing mantle minerals show only limited
269 variation in $\delta^{30}\text{Si}$ (-0.4 to -0.2) (e.g. Chakrabarti and Jacobsen, 2010; Savage et al., 2010),
270 but chemical weathering of silicates results in lighter Si isotopes being preferentially
271 sequestered into secondary clay minerals, which consequently display lower $\delta^{30}\text{Si}$ values
272 (Cornelis et al., 2010; Georg et al., 2007; Opfergelt et al., 2010; Ziegler et al., 2005). The
273 equilibrium Si isotope fractionation factor (for $\delta^{30}\text{Si}$) between kaolinite and quartz at
274 $\sim 27^\circ\text{C}$ is estimated at -1.6‰ (Meheut et al., 2007). Similarly, silica adsorbed on iron-
275 oxide/hydroxide particles preferentially incorporates the lighter Si isotopes, and
276 experimentally estimated fractionations (for $\delta^{30}\text{Si}$) range from ~ 1.1 ‰ for ferrihydrite and
277 ~ 1.6 ‰ for goethite; this process has been proposed as a possible explanation for ^{30}Si

278 depletion in soils (Delstanche et al., 2009; Opfergelt et al., 2009). The suspended load of
279 rivers typically has $\delta^{30}\text{Si}$ values similar to average igneous rocks and shales, whereas the
280 dissolved load in rivers show higher $\delta^{30}\text{Si}$ ($\sim +0.8$, this is about 1 to 1.2 ‰ higher than in
281 igneous rocks), a consequence of isotope mass balance after the precipitation of ^{30}Si -
282 depleted secondary minerals and soil formation (Ding et al., 2004; Georg et al., 2006a).
283 Groundwaters also show enrichment in the heavier isotopes of Si (Georg et al., 2009).
284 $\delta^{30}\text{Si}$ values for modern hydrothermal fluids from the East Pacific Rise (De la Rocha et
285 al., 2000) are, within analytical error, identical to those of terrestrial igneous rocks;
286 however, hydrothermal siliceous precipitates (e.g. from Mariana and Galapagos) show
287 very light $\delta^{30}\text{Si}$ (-0.4 to -3.1) similar to sinter deposits from continental hot springs (Ding
288 et al., 1996).

289 The mean $\delta^{30}\text{Si}$ of modern seawater is estimated at $\sim +1.1$, with both spatial and
290 depth variation in the seawater $\delta^{30}\text{Si}$ well-documented (De la Rocha et al., 2000). The
291 higher $\delta^{30}\text{Si}$ of modern seawater compared to the continental and hydrothermal Si inputs
292 reflects the preferential uptake of light Si isotopes by silica-secreting organisms,
293 particularly diatoms. Si isotope fractionation factors associated with biological uptake
294 range from ~ -1.1 ‰ for diatoms to -3.5 ‰ in marine sponges (e.g. De La Rocha, 2003; De
295 La Rocha et al., 1997; Varela et al., 2004; Beucher et al., 2008) (Table 2).

296

297 **5.2. Silica cycling and Si isotopes in Precambrian oceans**

298

299 Many of the same processes at work in the modern oceans were also present in
300 the Archean and Proterozoic eons, but biological diversity, redox conditions and the
301 relative strengths of erosional and hydrothermal fluxes all differed from today,
302 necessitating care in the interpretation of isotopic signatures. Silica fluxes are a corollary
303 of the alkalinity delivered to seawater by chemical weathering of the Earth's crust. The
304 sedimentary record of carbonate deposition reveals a pattern that is broadly similar over
305 Earth history (Grotzinger and James, 2000), reflecting long-term commonalities in
306 processes delivering carbon and alkalinity to seawater. Consequently, silica fluxes into
307 Precambrian oceans were likely similar to today, if not higher, given higher hydrothermal
308 fluxes (see below). Thus, silica must continually have left the oceans, and in the absence

309 of organisms producing siliceous skeletons, this occurred by means of physiochemical
310 processes. Without known biological processes to catalyze its removal, Precambrian
311 seawater was characterized by much higher concentrations of Si (Table 2), perhaps close
312 to amorphous silica saturation (Siever, 1991; Siever, 1992). Some silica must have been
313 incorporated into clays formed authigenically within sediments (e.g., Tosca et al., 2010).
314 Much, however, left the oceans as precipitates during evaporation of seawater and is
315 preserved primarily as early diagenetic cherts in shallow water carbonate successions
316 (Siever, 1992). Both chert precipitation and clay formation are accompanied by Si
317 isotopic fractionation, and so both processes should have led to enrichment of heavier Si
318 isotopes in ambient seawater.

319 Banded iron formations provide another significant but more temporally restricted
320 sink for silica. Iron formations generally contain 43-56% SiO₂ by weight (Klein, 2005)
321 and sedimentological evidence suggests that even BIF-cherts, similar to their shallow
322 water counterparts, form during diagenesis of precursor sediments. As most iron
323 formations, particularly those of Archean age, reflect off-shore, commonly basinal
324 deposition, silica precipitation was probably not forced by evaporation. Posth et al.
325 (2008) have suggested that the alternating Si and Fe deposition in BIFs is caused by
326 temperature fluctuations in the surface waters which slow down microbial iron mineral
327 formation but increase abiotic silica precipitation. While seasonal fluctuations in
328 saturation state might drive silica precipitation in shallow water, it is not clear that this
329 mechanism would work in the open marine settings where Archean iron formations
330 actually accumulated. Alternatively, silica may have been transported to deeper water
331 BIFs via the 'iron shuttle' (Fischer and Knoll, 2009) by adsorption on Fe-
332 oxide/hydroxide particles and accompanying Si isotope fractionation (c.f. Delstanche et
333 al., 2009) leading to the progressive enrichment of heavy Si isotopes in the ambient
334 water.

335 Finally, in Archean oceans, hydrothermal processes are thought to have played a
336 particularly important role in the marine silica cycle (see below). All of the relevant
337 sources and sinks (e.g.continental versus hydrothermal source) and processes (e.g.
338 evaporation, adsorption onto iron minerals, precipitation, and to some extent
339 transformation from one silica polymorph to another during diagenesis) make predictions

340 about the isotopic composition of ancient cherts. How might have they contributed to the
341 observed patterns of variation?

342

343 **5.3. Silica polymorphism, diagenesis, and its effect on Si isotope fractionation**

344

345 Studies of deep-sea sediments indicate that during diagenesis of siliceous ooze,
346 opal-A is transformed to opal-CT followed by chalcedony or cryptocrystalline quartz
347 (e.g. Kastner et al., 1977). To the best of our knowledge there are no detailed studies on
348 the effects of the above transformations on Si isotopic fractionation. The Si isotopic
349 compositions of Phanerozoic cherts (Fig. 2) overlap with those of modern diatoms and
350 siliceous sediments from black smokers (Robert and Chaussidon, 2006) suggesting that
351 very little isotopic fractionation has occurred with maturation of these siliceous sediments
352 although, closed-system experiments involving dissolution of diatom silica in seawater
353 suggests release of fluids with $\delta^{30}\text{Si}$ lower by $\sim 0.55\%$ compared to the starting material
354 (Demarest et al., 2009) (Table 2).

355 Ziegler et al. (2011) demonstrated that transformation of inorganic magadiite to
356 quartzose chert is not accompanied by any Si isotopic fractionation; in contrast, biogenic
357 marine opal from the Monterey Formation is offset in $\delta^{30}\text{Si}$ from the cristobalitic Monterey
358 chert by 1.4% . However, the latter offset is thought to be an imprint of a later diagenetic
359 fluid and not necessarily due to transformation of opal-A to cristobalitic chert.

360 As observed in silcretes (Basile-Doelsch et al., 2005), terrestrial amorphous silica
361 precipitates are isotopically lighter than the ambient fluid. However, the Si isotope
362 fractionation factor between amorphous silica precipitates and water remains to be
363 determined accurately, and may vary as a function of the precipitation mechanism as well
364 as setting. For example, in contrast to terrestrial pedogenic and groundwater silcretes,
365 where later-formed macro-crystalline quartz is depleted in ^{30}Si compared to the early-
366 formed micro-crystalline quartz or the original detrital quartz, no isotopic fractionation
367 has been observed between detrital quartz and microcrystalline quartz during marine
368 silicification (Basile-Doelsch et al., 2005). Overall, while it may be expected that silica
369 polymorph transformations, which involve dissolution and reprecipitation, might be

370 accompanied by Si isotopic fractionation, there is no strong evidence for this actually
371 compromising isotopic measurements.

372

373 **5.4. Temporal variation of $\delta^{30}\text{Si}$ in Precambrian cherts**

374

375 Precambrian cherts show a large range in $\delta^{30}\text{Si}$; this is clear from both our
376 measurements of Late Archean and Proterozoic cherts (Fig. 2), other MC-ICPMS data
377 from Archean samples (Abraham et al., 2011; Andre et al., 2006; Steinhoefel et al., 2009,
378 2010; van den Boorn et al., 2007, 2010) as well as in-situ analyses (Robert and
379 Chaussidon, 2006; Heck et al., 2011).

380 We explain the temporal variation in $\delta^{30}\text{Si}$ in Precambrian cherts in light of: 1)
381 simple mixing of silica derived from continental and hydrothermal sources, 2)
382 mechanisms of silica precipitation and 3) equilibrium and Rayleigh-type fractionation
383 within a single basin associated with early diagenesis.

384

385 *5.4.1. Silica fluxes to the Precambrian oceans and their isotopic composition:*

386 In the modern day, $\delta^{30}\text{Si}$ of the continental Si flux (dissolved load in rivers) is
387 distinctly higher than that of the hydrothermal flux (hydrothermal fluids) (Table 2). It is
388 reasonable to assume that the $\delta^{30}\text{Si}$ of hydrothermal fluids remained unchanged even in
389 Precambrian ocean basins, even though magnitude of the hydrothermal flux to the oceans
390 may have been different. $\delta^{30}\text{Si}$ of the continental input, however, could have varied in the
391 past as a result of varying rates of chemical weathering or the presence of Fe^{2+} in the soil
392 prior to the rise of oxygen.

393 Van den Boorn et al. (2007, 2010) categorized early Archean cherts into two
394 types with contrasting silica sources based on petrography, trace element concentration
395 patterns, and Si isotopic composition. Their “C-cherts,” with abundant iron hydroxides,
396 minor carbonates and sulfides, positive Eu, La and Y anomalies, depletion in lithophile
397 trace elements, and relatively large range in $\delta^{30}\text{Si}$ (-2.4 to +1.1), are interpreted as
398 orthochemical primary precipitates derived from either hydrothermal fluids or mixtures
399 of hydrothermal fluids and seawater. Their “S-cherts” contain sericite, Ti-oxides and
400 some zircon, lack REE+Y anomalies, are enriched in lithophile elements, show a

401 restricted range in $\delta^{30}\text{Si}$ (+0.1 to +1.1) and are inferred to have formed by silicification of
402 volcanogenic sediments, with the excess silica derived only from seawater.

403 We can reflect on this hypothesis with estimates of continental and hydrothermal
404 fluxes to the ancient oceans based on other geochemical and isotopic proxies. Nd isotopic
405 signatures of Precambrian BIFs reveal that the REE budget of the Archean and early
406 Proterozoic oceans (older than ~ 1.9 Ga) was dominated by hydrothermal fluids
407 circulating through mid-oceanic ridges (Jacobsen and Pimentel-Klose, 1988a, b),
408 although locally shallow water masses may have maintained distinctly unradiogenic Nd
409 isotopic composition, as observed in the ~ 2.9 Ga old Mozaan BIFs (Alexander et al.,
410 2009). In contrast, the Nd isotopic composition of BIFs in the younger Paleoproterozoic
411 Gunflint Formation and Neoproterozoic Urucum Formation indicate a dominantly
412 continental source for the REEs (Jacobsen and Pimentel-Klose, 1988b). Fe/Nd ratios
413 indicate that the predominant source of Fe in Archean and early Proterozoic BIFs and for
414 seawater in general was hydrothermal (Jacobsen and Pimentel-Klose, 1988a, b).

415 REEs (Bau and Dulski, 1996; Derry and Jacobsen, 1990) support the inference
416 from Nd isotope data and suggest that Fe and REEs derived from submarine
417 hydrothermal systems co-precipitated from seawater as Fe-oxy-hydroxides in precursor
418 sediments to BIFs. Seawater Sr isotopic composition shows a change from mantle-like
419 $^{87}\text{Sr}/^{86}\text{Sr}$ before 2.5 Ga towards increasingly radiogenic $^{87}\text{Sr}/^{86}\text{Sr}$ afterward (Shields and
420 Veizer, 2002). The shift towards more radiogenic Sr and less radiogenic Nd near the
421 Archean-Proterozoic boundary is thought to reflect a change from a “mantle”-buffered
422 to a “continent”-buffered global seawater composition around this time and is likely to
423 result from a combination of decreasing heat flux from the mantle and intensified
424 formation of continental crust. However, Si isotopic variability in Precambrian cherts do
425 not show any dramatic change from low $\delta^{30}\text{Si}$, akin to hydrothermal sources, to higher
426 values (similar to the dissolved load in rivers) at around 2.5 Ga (Fig 2). One possibility is
427 that estimating continental and hydrothermal fluxes based on REE concentration patterns
428 or Nd and Sr isotopes might not be directly applicable to Si. In the modern oceans, while
429 REE concentrations increase with depth, they are not correlated with Si concentrations,
430 suggesting a decoupling between the REE cycle and the Si cycle. REE concentrations
431 continue to increase with depth even after Si and PO_4^{3-} have reached their deep-water

432 maxima (Piegras and Jacobsen, 1992). However, this decoupling could be due to the
433 effect of organisms on Si concentration and might not be applicable to the Precambrian.
434 Si concentrations, however, co-vary with the Nd isotopic composition of Pacific bottom
435 water and follow a mixing trend (Piegras and Jacobsen, 1988).

436 In contrast to REE and Nd isotope studies, Ge/Si measurements of the silica rich
437 layers in BIF from the 2.5 Ga old Dales Gorge Member of the Hamersley Group suggest
438 that silica in these BIFs was derived by weathering of continental land mass, whereas the
439 iron has a hydrothermal origin (Hamade et al., 2003). However, this hypothesis requires
440 that chemical precipitation of silica does not fractionate Ge from Si and that the Ge/Si
441 ratio of continental and hydrothermal sources has remained constant over time. This does
442 not appear to be the case (Anders et al., 2003; Fischer and Knoll, 2009; Hammond et al.,
443 2000; Pokrovsky et al., 2006). In addition, it is not clear how the Ge/Si ratio is affected
444 by diagenesis (Hamade et al., 2003).

445 Clearly, temporal variations of $\delta^{30}\text{Si}$ in cherts cannot be explained solely by
446 simple mixing of isotopically distinct continental and hydrothermal sources, unlike
447 seawater Nd and Sr isotope variations over time. Additional mechanisms need to be
448 invoked; these are discussed below.

449

450 *5.4.2. Mechanism of silica precipitation:*

451 Cherts associated with iron formations tend to have lower $\delta^{30}\text{Si}$ values than non-
452 BIF peritidal cherts, even in the same basin (Fig. 2, 3). For example, within the Late
453 Archean Transvaal basin, peritidal cherts tend to be at least 1‰ higher in $\delta^{30}\text{Si}$ than BIF
454 cherts deposited at depth. This is consistent with the hypothesis of hydrothermal versus
455 continental origins of silica (Andre et al., 2006; Steinhoefel et al., 2009; Steinhoefel et al.,
456 2010; Heck et al., 2011) We postulate that $\delta^{30}\text{Si}$ in Precambrian cherts not only reflects
457 the source of silica but also the depositional conditions and the mechanism by which
458 silica was precipitated.

459 The relatively low Si-isotopic values of cherts in iron formation could reflect
460 deposition by adsorption onto Fe-oxide/hydroxide particles consistent with observations
461 from laboratory experiments (Delstanche et al., 2009). Silica adsorption onto iron
462 oxides/hydroxides would also have occurred in soils following the initial oxygenation of

463 the atmosphere and surface ocean 2.3-2.45 Ga (Holland, 2006), resulting in a higher $\delta^{30}\text{Si}$
464 of continental silica entering the oceans.

465 Thus, in concert, changing hydrothermal fluxes into the oceans and Earth's
466 evolving redox state provide a reasonable first order explanation for the observed
467 increase in chert $\delta^{30}\text{Si}$ values from early Archean through mid-Proterozoic time. These
468 factors may also explain the observed decrease in mean $\delta^{30}\text{Si}$ values for Neoproterozoic
469 cherts. This explanation is consistent with Sr isotopic studies which suggest reinvigorated
470 hydrothermal influence on seawater in association with Neoproterozoic continental
471 breakup (e.g., Asmerom et al., 1991; Halverson et al., 2007), and Fe speciation analyses
472 which indicate a return to ferruginous subsurface water masses at this time (Johnston et
473 al., 2010), if not earlier (Planavsky et al., 2011).

474 Against this backdrop, the remarkably low $\delta^{30}\text{Si}$ of the oolitic iron formation of
475 the Paleoproterozoic Frere Formation (-2.68), Western Australia, and basinal cherts
476 associated with the possibly coeval Duck Creek Formation (-4.29), Western Australia,
477 deserve special mention. Although such low $\delta^{30}\text{Si}$ values are rare in our dataset, similarly
478 values have been reported in BIFs from Isua and the Transvaal craton and explained as
479 hydrothermally derived Si that has been further fractionated by adsorption on to Fe-
480 hydroxide as well as later crystallization (Heck et al., 2011). Such an explanation may
481 well apply to our late Paleoproterozoic samples, consistent with the hypothesis that this
482 resurgence of iron formation after several hundred years' absence reflects a superplume
483 (Condie, 2004).

484

485 *5.4.3. Si isotopic variation in peritidal cherts from individual basins*

486 Si-isotopic values within the late Archean Transvaal basin vary by nearly 3‰,
487 explainable, at least in part, by differences between peritidal and basin BIF cherts. The 25
488 chert samples measured from the ~750-800 Ma old Akademikerbreen Group,
489 Spitsbergen, and its correlatives in Nordaustlandet and East Greenland, show a
490 comparable range of $\delta^{30}\text{Si}$ values from -1.78 to +1.26. For the latter sample set, however,
491 another explanation is required to explain the observed variation, as all come from early
492 diagenetic cherts within peritidal carbonate facies.

493 Variation in $\delta^{30}\text{Si}$ in the Spitsbergen cherts can be explained by fractionation
494 during precipitation from silica-saturated porewaters. The $\delta^{30}\text{Si}$ evolution of the
495 precipitates and the fluid can be modeled for both a closed system (i.e. precipitate is in
496 equilibrium with the ambient fluid) and an open system (Rayleigh fractionation, i.e.
497 precipitate is removed from the system) using standard equations (c.f. Criss, 1999) and
498 are shown in Figure 4. The Si isotope fractionation factor between silica saturated fluids
499 and silica precipitating from them is not well constrained although it is known that
500 chemical precipitates preferentially incorporate the lighter Si isotopes (e.g. Basile-
501 Doelsch et al., 2005). In this model, the fractionation between the fluid (silica saturated
502 porewater) and the precipitate (cherts), which increases with decreasing temperature, is
503 such that in Case 1 the precipitate is 2.0 ‰ lower than the fluid and in Case 2 it is 3.0 ‰
504 lower. The initial $\delta^{30}\text{Si}$ of the fluid is assumed to be 0.8 ‰, similar to the $\delta^{30}\text{Si}$ of modern
505 dissolved load in rivers. Although the absolute values of the fractionation factors are
506 arbitrarily chosen, they are consistent with fractionations in other natural systems (Table
507 2). Using the above parameters, the entire range in $\delta^{30}\text{Si}$ in the Spitsbergen cherts (~3‰)
508 can be explained by a Rayleigh-type isotope fractionation with f ranging from 1 to 0.2.
509 Fractionations are much smaller for the equilibrium/closed-system scenario. The $\delta^{30}\text{Si}$
510 range in cherts at any instant of time could be explained by a similar mechanism. Thus
511 we interpret the large range of values in the peritidal cherts as being due to fractional
512 crystallization of the silicifying fluid that replaced the initial limestones with cherts.

513 We also consider the effect of early-diagenesis on the Si isotopic composition of
514 amorphous siliceous precipitates as some of our samples show indications of later
515 diagenetic modification. As discussed in Section 5.2, transformation from amorphous
516 opal-A to micro-crystalline quartz involves dissolution and reprecipitation which is
517 expected to be accompanied by Si isotope fractionation, although there is no convincing
518 evidence thus far for such an effect. Nevertheless, it has been observed that dissolution of
519 biogenic opal in seawater releases light isotopes of Si ($\delta^{30}\text{Si}$ light by 0.5 ‰) (Demarest et
520 al., 2009) while precipitates also favor the light Si isotopes (e.g. Basile-Doelsch et al.,
521 2005). Hence, the net isotope fractionation between silica saturated porewaters and chert
522 can be considered as an additive effect of precipitation and continued dissolution and
523 could contribute to the large $\delta^{30}\text{Si}$ range in cherts at any instant of time.

524 The high Si content in cherts makes Si isotopic composition of cherts less
525 susceptible to pervasive post-depositional changes (e.g. Heck et al., 2011, Marin-
526 Carbonne et al., 2011). This is consistent with the large variations observed in peritidal
527 cherts; any pervasive late-stage modification would have resulted in a more uniform Si
528 isotopic composition in these samples. This conclusion is consistent with recent in-situ
529 measurements of Si isotopes in Archean BIFs (Heck et al., 2011).

530

531 **5.5. Toward understanding the temporal variation in the Si isotopic composition of** 532 **Precambrian seawater**

533

534 The isotopic composition of ancient seawater can be reconstructed from analyses
535 of chemical precipitates derived from seawater (e.g. Shields and Veizer, 2002). However,
536 post-depositional alteration often obliterates the pristine seawater isotopic signature as
537 observed in Sr, C and O isotopic studies of carbonates; the extent to which post-
538 depositional overprinting occurs depends on the concentration of the element in the rock
539 versus the diagenetic fluid (c.f. Jacobsen and Kaufman, 1999). It has been argued that the
540 low permeability of cherts make them less prone to late-dissolution/reprecipitation events
541 compared to carbonates and low water/rock ratios during metamorphic heating does not
542 result in perturbation of $\delta^{18}\text{O}$ in cherts (c.f. Knauth, 2005). $\delta^{18}\text{O}$ in Precambrian cherts
543 show a gradual change from ^{18}O -depleted values in the Archean to more enriched values
544 in the Neoproterozoic. This is been interpreted to reflect warm ocean waters (55-85 °C) in
545 the Archean to cooler temperatures with time (Knauth, 2005 and references therein,
546 Marin et al., 2010). Based on an observed positive correlation between Si and O isotopic
547 values in Precambrian cherts, Robert and Chaussidon (2006) interpreted secular
548 variations in Si-isotopic composition of seawater in terms of a single reservoir with a
549 single silica source from weathering and two sinks, sedimentary rocks and hydrothermal
550 alteration of the crust, respectively. Given knowledge of the isotope fractionation during
551 hydrothermal silicification (admittedly poorly constrained) and measurements of the
552 isotopic composition of the sedimentary sink, this system can be solved for the fraction of
553 silica that departs in the sedimentary sink; if correct, this framework provides the logic
554 for a proxy of seawater temperature (due to the temperature dependence of amorphous

555 silica solubility) (Robert and Chaussidon, 2006) similar to oxygen isotopes. However, it
556 is difficult to characterize the sedimentary Si flux with any single $\delta^{30}\text{Si}$ value as discussed
557 before, complicating the hypothesis of Robert and Chaussidon (2006). While it is
558 possible that O isotopes in Archean cherts reflect warm temperatures, the temperatures
559 are warm because the ambient waters were hydrothermal, not seawater (e.g., Blake et al.,
560 2010; Pope et al., 2012). To the extent that this is the case, Si and O isotopes might
561 covary in Archean cherts not because they both record seawater T but because both
562 reflect declining hydrothermal input through time.

563 The Si isotopic composition of seawater at any given moment in the Precambrian
564 was likely a function of the Si isotopic composition of continental and hydrothermal
565 inputs and outputs (peritidal chert precipitation and BIF formation), their relative fluxes,
566 and the isotopic fractionation factors related to precipitation of silica from seawater or
567 porewater ($\Delta_{SW-chert}$) and/or adsorption of silica onto Fe-hydroxide particles during BIF
568 formation (Δ_{SW-BIF}). Given the long residence time of Si relative to mixing times of the
569 ocean (Table 2), it is likely that Si in Precambrian cherts was derived from seawater with
570 relatively uniform Si isotope composition. Hence, $\delta^{30}\text{Si}$ variations in cherts over time
571 may indirectly reflect the temporal variation of $\delta^{30}\text{Si}$ of the seawater. As discussed above,
572 $\delta^{30}\text{Si}$ of chemical precipitates (e.g. cherts) tend to be lower than that of the ambient
573 solution (e.g. seawater or porewater). In addition, the fractionations associated with
574 various Si sources and sinks may have changed or been differentially expressed
575 throughout Proterozoic time (e.g. during times of banded iron formation deposition or
576 enhanced authigenic clay formation). In the absence of well-constrained fractionation
577 factors, we present a qualitative analysis of factors that can cause variation in the
578 seawater $\delta^{30}\text{Si}$.

579 Let us first consider a simple case, where the continental and hydrothermal Si
580 fluxes to the ocean, their isotopic compositions as well as the isotopic fractionation
581 factors during chert and BIF formation remain constant over Earth history. Even with a
582 significant fractionation during precipitation, the isotopic composition of cherts would
583 show no variation with time. However, if the relative contributions of continental and
584 hydrothermal fluxes of silica to the oceans varied over time as suggested by Nd isotopes

585 (e.g. Jacobsen and Pimentel-Klose, 1988a,b), the $\delta^{30}\text{Si}$ variation in cherts from 3.8 Ga to
586 1.5 Ga may reflect a gradual change from hydrothermal to continental silica sources. If
587 correct, this would suggest an important change in the locus of silicate weathering during
588 Proterozoic time.

589 Additionally, the silicon isotopic composition of the continental flux could also
590 have varied with time. Increased clay genesis during soil formation, including
591 interactions of Si with ferric oxides after the rise of atmospheric oxygen, would result in
592 preferential removal of light Si on particles, and an increase in the $\delta^{30}\text{Si}$ of the dissolved
593 load in rivers ultimately delivered to the oceans. Extent of silica depletion as well as
594 wetter versus drier climates can also alter soil $\delta^{30}\text{Si}$ (Bern et al., 2010). These processes
595 could also explain the high $\delta^{30}\text{Si}$ in Mid-Proterozoic cherts, which is a prominent feature
596 in both our dataset and that of Robert and Chaussidon (2006).

597 The reversal in the above trend towards lower $\delta^{30}\text{Si}$ since 1.5 Ga is harder to
598 explain. One possibility is an increased flux of light hydrothermal source-derived Si into
599 the oceans associated with Neoproterozoic breakup of Rodinia (e.g. Dalziel, 1997; Evans,
600 2009; Pisarevsky et al., 2003). However, this does not explain why values begin to
601 decline as early as 1.2 Ga. Moreover, other isotopic proxies of paleo-seawater
602 composition like Nd, Sr isotopes do not show any evidence of an increased hydrothermal
603 flux of Si (low $\delta^{30}\text{Si}$) beginning 1.5 Ga ago. Alternatively, the disappearance of BIFs
604 (very low $\delta^{30}\text{Si}$) at ~1.8 Ga would leave the ambient seawater relatively less enriched in
605 the heavier Si isotopes and this would be reflected in lower $\delta^{30}\text{Si}$ in peritidal cherts
606 precipitating from this seawater. The timing of the general disappearance of iron
607 formation deposits from the sedimentary record, however, occurs several hundred million
608 years too early to easily satisfactorily explain this trend. Moreover, continued
609 precipitation of cherts (low $\delta^{30}\text{Si}$) would result in progressively higher $\delta^{30}\text{Si}$ in younger
610 cherts, which is in contrast to the observed trend.

611 The decreasing $\delta^{30}\text{Si}$ trend in cherts since 1.5 Ga ago continues into the
612 Phanerozoic, even though the marine silica cycle changed drastically in the Phanerozoic
613 due to evolution of silica secreting organisms, which preferentially take up the lighter
614 isotopes of Si. In the presence of silica secreting organisms, the seawater $\delta^{30}\text{Si}$ and hence

615 that of cherts precipitating from it should have been higher in the Phanerozoic than what
616 is observed (Fig 2). This suggests that abiotic mechanisms, similar to the ones discussed
617 above, may be the dominant drivers of the Si isotopic composition of the seawater over
618 time.

619

620 **6. CONCLUSIONS**

621

622 We have presented the first high-precision MC-ICPMS measurements of the Si
623 isotopic composition of Proterozoic cherts. These samples, collected from a wide range
624 of sedimentary settings from different parts of the world, show large variations in $\delta^{30}\text{Si}$,
625 from +2.85 to -4.29. These trends reflect, in part, variable contributions between
626 isotopically distinct hydrothermal and continental sources of silica to seawater.
627 Additionally, $\delta^{30}\text{Si}$ variability reflects clear paleoenvironmental differences in chert
628 petrogenesis, including the redox profile of ambient ocean basins. In combination with
629 other available MC-ICPMS measurements of Precambrian cherts, our data indicate that
630 peritidal cherts, formed by early diagenetic replacement of carbonates, show relatively
631 high $\delta^{30}\text{Si}$ compared to basinal cherts associated with BIFs. We suggest that such
632 contrasting $\delta^{30}\text{Si}$ in cherts reflect the mechanisms of silica precipitation. Shallow water
633 cherts precipitate out of silica-saturated porewaters, primarily driven by evaporation,
634 whereas silica in basinal cherts associated with BIFs was transported to deeper waters by
635 adsorption onto Fe-hydroxide particles. Laboratory experiments showing that silica
636 adsorption onto Fe-hydroxide particles preferentially deposits lighter Si isotopes is
637 consistent with the relatively low $\delta^{30}\text{Si}$ observed in BIFs. Additionally, the lower $\delta^{30}\text{Si}$ in
638 BIFs could also reflect Si being primarily derived from hydrothermal sources. The large
639 variation in $\delta^{30}\text{Si}$ of peritidal cherts from a single basin can be explained by Rayleigh-
640 type fractionation during precipitation from silica-saturated porewaters. There is no
641 evidence thus far to suggest that silica polymorph transformation during chert formation
642 results in significant Si isotope fractionation. Post-depositional dissolution and
643 reprecipitation of silica could have contributed to the large range in $\delta^{30}\text{Si}$ in a single basin
644 but high silica in cherts makes $\delta^{30}\text{Si}$ values less susceptible to pervasive post-depositional
645 changes.

646 Despite differential fractionations due to paleoenvironmental differences and
647 precipitation processes, the global dataset shows a broad pattern of temporal variability.
648 $\delta^{30}\text{Si}$ increase monotonically from 3.8 Ga to 1.5 Ga, attributed to varying continental
649 versus hydrothermal silica fluxes to the oceans as well as isotopic fractionation related to
650 precipitation of cherts and BIFs. A Mesoproterozoic $\delta^{30}\text{Si}$ maxima observed in 1.5 Ga old
651 peritidal cherts may reflect an increase in Si isotope fractionation during soil forming
652 processes (possibly related to higher atmospheric oxygen concentrations and more ferric
653 iron in soil horizons) which increased the $\delta^{30}\text{Si}$ of the dissolved load of rivers and
654 consequently seawater. The causes behind decreasing $\delta^{30}\text{Si}$ in cherts from 1.5 Ga onward
655 remain unclear. However this trend continues into Phanerozoic time, suggesting an
656 underlying similarity in the dominant factors controlling the silicon isotopic composition
657 of seawater through the later Proterozoic and Phanerozoic eons.

658

659 *Acknowledgements:* This work was supported by NASA Cosmochemistry Program grants
660 #NNX07AF86G #NNX10AI43G to SBJ. RC thanks the Origins of Life Initiative at
661 Harvard University for his post-doctoral support. AHK and WWF thank the Agouron
662 Institute and AHK thanks the NASA Astrobiology Institute for support. We thank Dr.
663 Philipp Heck and two other anonymous reviewers and the Associate Editor Dr. Clark
664 Johnson for their comments and suggestions.

665

666 REFERENCES

- 667 Abraham, K., Hofmann, A., Foley, S.F., Cardinal, D., Harris, C., Barth, M.G., and Andre,
668 L. (2011) Coupled silicon-oxygen isotope fractionation traces Archaean
669 silicification. *Earth Planet. Sci. Lett.* **301**, 222-230.
- 670 Alexander, B.W., Bau, M., and Andersson, P. (2009) Neodymium isotopes in Archean
671 seawater and implications for the marine Nd cycle in Earth's early oceans. *Earth*
672 *Planet. Sci. Lett.* **283**, 144-155.
- 673 Allison, C. W., and Awramik, S.M. (1989) Organic-walled microfossils from earliest
674 Cambrian or latest Proterozoic Tinder Group rocks, Northwest Canada.
675 *Precamb. Res.* **43**, 253-294.

676 Anders, A.M., Sletten, R.S., Derry, L.A., and Hallet, B. (2003) Germanium/silicon ratios
677 in the Copper River Basin, Alaska: Weathering and partitioning in periglacial
678 versus glacial environments. *J. Geophys. Res.* **108**, 6005, doi:
679 10.1029/2003JF000026.

680 Andre, L., Cardinal, D., Alleman, L.Y., and Moorbath, S., 2006, Silicon isotopes in 3.8
681 Ga West Greenland rocks as clues to the Eoarchaeon supracrustal Si cycle. *Earth*
682 *Planet. Sci. Lett.* **245**, 162-173.

683 Asmerom, Y., Jacobsen, S.B., Knoll, A.H., Butterfield, N.J., and Swett, K., 1991,
684 Strontium Isotopic Variations of Neoproterozoic Seawater - Implications for
685 Crustal Evolution. *Geochim. Cosmochim. Acta* **55**, 2883-2894.

686 Barghoorn, E.S., and Tyler, S.A. (1965) Microorganisms from the Gunflint Chert.
687 *Science* **147**, 563-577.

688 Basile-Doelsch, I., Meunier, J.D., and Parron, C. (2005) Another continental pool in the
689 terrestrial silicon cycle. *Nature* **433**, 399-402.

690 Bau, M., and Dulski, P. (1996), Distribution of yttrium and rare-earth elements in the
691 Penge and Kuruman iron-formations, Transvaal Supergroup, South Africa.
692 *Precamb. Res.* **79**, 37-55.

693 Bern, C. R., Brzezinski, M. A., Beucher, C., Ziegler, K., and Chadwick, O. A. (2010)
694 Weathering, dust, and biocycling effects on soil silicon isotope ratios. *Geochim.*
695 *Cosmochim. Acta* **74**, 876-889. Beucher, C. P., Brzezinski, M. A., and Jones, J. L.,
696 (2008), Sources and biological fractionation of Silicon isotopes in the Eastern
697 Equatorial Pacific. *Geochim. Cosmochim. Acta* **72**, 3063-3073.

698 Blake, R.E., Chang, S.J., and Lepland, A. (2010) Phosphorus oxygen isotope evidence for
699 a temperate and biologically active Archean ocean. *Nature* **464**, 1029-1232.

700 Brotton, S. J., Shapiro, R., van der Laan, G., et al. (2007) Valence state fossils in
701 Proterozoic stromatolites by L-edge X-ray absorption spectroscopy. *Jour.*
702 *Geophys. Res. Biogeosc.* **112**, G03004 DOI: 10.1029/2006JG000185.

703 Chakrabarti, R., and Jacobsen, S.B. (2010) Silicon isotopes in the inner Solar System:
704 Implications for core formation, solar nebular processes and partial melting.
705 *Geochim. Cosmochim. Acta* **74**, 6921-6933.

706 Condie, K.C. (2004) Supercontinents and superplume events: distinguishing signals in
707 the geologic record. *Physics Earth Planet. Int.* **146**, 319-332.

708 Cornelis, J.T., Delvaux, B., Cardinal, D., Andre, L., Ranger, J., and Opfergelt, S. (2010)
709 Tracing mechanisms controlling the release of dissolved silicon in forest soil
710 solutions using Si isotopes and Ge/Si ratios. *Geochim. Cosmochim. Acta.* **74**,
711 3913-3924.

712 Criss, R. E. (1999) *Principles of Stable Isotope Distribution*. New York, Oxford
713 University Press.

714 Dalziel, I. W. D. (1997) Neoproterozoic-Paleozoic geography and tectonics: Review,
715 hypothesis, environmental speculation. *Geological Society of America Bulletin*
716 **109**, 16-42.

717 Dawes, P.R. (1997) The Proterozoic Thule Supergroup, Greenland and Canada: history,
718 lithostratigraphy and development. *Greenland Geological Survey Bulletin* **174**, 1-
719 150.

720 De La Rocha, C.L. (2003) Silicon isotope fractionation by marine sponges and the
721 reconstruction of the silicon isotope composition of ancient deep water. *Geology*
722 **31**, 423-426.

723 De La Rocha, C.L., Brzezinski, M.A., and DeNiro, M.J. (1997) Fractionation of silicon
724 isotopes by marine diatoms during biogenic silica formation. *Geochim.*
725 *Cosmochim. Acta* **61**, 5051-5056.

726 De la Rocha, C.L., Brzezinski, M.A., and DeNiro, M.J. (2000) A first look at the
727 distribution of the stable isotopes of silicon in natural waters. *Geochim.*
728 *Cosmochim. Acta* **64**, 2467-2477.

729 Delstanche, S., Opfergelt, S., Cardinal, D., Elsass, F., Andre, L., and Delvaux, B. (2009)
730 Silicon isotopic fractionation during adsorption of aqueous monosilicic acid onto
731 iron oxide. *Geochim. Cosmochim. Acta* **73**, 923-934.

732 Demarest, M. S., Brzezinski, M. A., and Beucher, C. P. (2009) Fractionation of silicon
733 isotopes during biogenic silica dissolution. *Geochim. Cosmochim. Acta* **73**, 5572-
734 5583.

- 735 Derry, L.A., and Jacobsen, S.B. (1990) The Chemical Evolution of Precambrian Seawater
736 - Evidence from Rees in Banded Iron Formations. *Geochim. Cosmochim. Acta* **54**,
737 2965-2977.
- 738 Ding, T., Jiamg, S., Wan, D., Li, Y., Li, J., Song, H., Liu, Z., and Yao, X. (1996) *Silicon*
739 *isotope geochemistry*. Beijing, China, Geological Publishing House.
- 740 Ding, T., Wan, D., Wang, C., and Zhang, F. (2004) Silicon isotope compositions of
741 dissolved silicon and suspended matter in the Yangtze River, China. *Geochim.*
742 *Cosmochim. Acta* **68**, 205-216.
- 743 Evans, D.A.D. (2009). The palaeomagnetically viable, long-lived and all-inclusive
744 Rodinia supercontinent reconstruction. In *Ancient Orogens and Modern*
745 *Analogues* (eds. J. B. Murphy, J. D. Keppie and A. Hynes), Geological Society of
746 London Special Publication 327, pp 371-404.
- 747 Fischer, W.W., and Knoll, A.H. (2009) An iron shuttle for deepwater silica in Late
748 Archean and early Paleoproterozoic iron formation. *Geological Society of*
749 *America Bulletin* **121**, 222-235.
- 750 Georg, R.B., Reynolds, B.C., Frank, M., and Halliday, A.N. (2006a) Mechanisms
751 controlling the silicon isotopic compositions of river waters. *Earth Planet. Sci.*
752 *Lett.* **249**, 290-306.
- 753 Georg, R.B., Reynolds, B.C., Frank, M., and Halliday, A.N. (2006b) New sample
754 preparation techniques for the determination of Si isotopic compositions using
755 MC-ICPMS. *Chem. Geol.* **235**, 95-104.
- 756 Georg, R.B., Reynolds, B.C., West, A.J., Burton, K.W., and Halliday, A.N. (2007)
757 Silicon isotope variations accompanying basalt weathering in Iceland. *Earth*
758 *Planet. Sci. Lett.* **261**, 476-490.
- 759 Georg, R.B., West, A.J., Basu, A.R., and Halliday, A.N. (2009) Silicon fluxes and isotope
760 composition of direct groundwater discharge into the Bay of Bengal and the effect
761 on the global ocean silicon isotope budget. *Earth Planet. Sci. Lett.* **283**, 67-74.
- 762 Green, J.W., Knoll, A.H., and Swett, K. (1989) Microfossils from silicified stromatolitic
763 carbonates of the Upper Proterozoic Limestone-Dolomite 'Series', central East
764 Greenland. *Geol. Mag.* **126**, 567-585.

765 Grotzinger, J.P., and James, N.P. (2000) Precambrian carbonates: evolution of
766 understanding, In *Carbonate Sedimentation and Diagenesis in the Evolving*
767 *Precambrian World* (eds. J. P. Grotzinger and N. P. James), SEPM Special
768 Publication 67, Tulsa, OK, pp. 3-20.

769 Halverson, G.P., Dudas, F.O., Maloof, A.C., and Bowring, S.A. (2007) Evolution of the
770 $^{87}\text{Sr}/^{86}\text{Sr}$ composition of Neoproterozoic seawater. *Palaeogeography*
771 *Palaeoclimatology Palaeoecology* **256**, 103-129.

772 Hamade, T., Konhauser, K.O., Raiswell, R., Goldsmith, S., and Morris, R.C. (2003)
773 Using Ge/Si ratios to decouple iron and silica fluxes in Precambrian banded iron
774 formations. *Geology* **31**, 35-38.

775 Hammond, D.E., McManus, J., Berelson, W.M., Meredith, C., Klinkhammer, G.P., and
776 Coale, K.H. (2000) Diagenetic fractionation of Ge and Si in reducing sediments:
777 The missing Ge sink and a possible mechanism to cause glacial/interglacial
778 variations in oceanic Ge/Si. *Geochim. Cosmochim. Acta* **64**, 2453-2465.

779 Heck, P. R., Huberty, J. M., Kita, N. T., Ushikubo, T., Kozdon, R., Valley, J. W. (2011)
780 SIMS analyses of silicon and oxygen isotope ratios for quartz from Archean and
781 Paleoproterozoic banded iron formations. *Geochim. Cosmochim. Acta* **75**, 5879-
782 5894.

783 Holland, H.D. (2006) The oxygenation of the atmosphere and oceans. *Phil. Trans. Royal*
784 *Soc. B* **361**, 903-915.

785 Jacobsen, S.B., and Pimentel-Klose, M.R. (1988a) A Nd Isotopic Study of the Hamersley
786 and Michipicoten Banded Iron Formations - the Source of REE and Fe in Archean
787 Oceans. *Earth Planet. Sci. Lett.* **87**, 29-44.

788 Jacobsen, S.B., and Pimentel-Klose, M.R. (1988b) Nd Isotopic variations in Precambrian
789 Banded Iron Formations. *Geophys. Res. Lett.* **15**, 393-396.

790 Jacobsen, S.B., and Kaufman, A. J. (1999) The Sr, C and O isotopic evolution of
791 Neoproterozoic seawater. *Chem. Geol.* **161**, 37-57.

792 Johnston, D.T., Poulton, S.W., Dehler, C., Porter, S., Husson, J., Canfield, D.E., and
793 Knoll, A.H. (2010) An emerging picture of Neoproterozoic ocean chemistry:
794 Insights from the Chuar Group, Grand Canyon, USA. *Earth Planet. Sci. Lett.* **290**,
795 64-73.

- 796 Kah, L.C., and Knoll, A.H. (1996) Microbenthic distribution of proterozoic tidal flats:
797 Environmental and taphonomic considerations. *Geology* **24**, 79-82.
- 798 Kastner, M., Keene, J. B., Gieskes, J. M. (1977) Diagenesis of siliceous oozes - I.
799 Chemical controls on the rate of opal-A to opal-CT transformation - an
800 experimental study. *Geochim. Cosmochim. Acta* **41**, 1041-1059.
- 801 Klein, C. (2005) Some Precambrian banded iron-formations (BIFs) from around the
802 world: Their age, geologic setting, mineralogy, metamorphism, geochemistry, and
803 origin. *American Mineralogist* **90**, 1473-1499.
- 804 Knauth, L. P. (2005) Temperature and salinity history of the Precambrian ocean:
805 implications for the course of microbial evolution. *Paleogeog. Paleoclim.*
806 *Paleoecol.* **219**, 53-69.
- 807 Knoll, A. (1985) Exceptional preservation of photosynthetic organisms in silicified
808 carbonates and silicified peats. *Phil. Trans. Royal Soc. London* **311**, 11-122.
- 809 Knoll, A.H. (1984) Microbiotas of the late Precambrian Hunnberg Formation,
810 Nordaustlandet, Svalbard. *Journal of Paleontology* **58**, 131-162.
- 811 Knoll, A.H., and Beukes, N.J. (2009) Introduction: Initial investigations of a Neoproterozoic
812 shelf margin-basin transition (Transvaal Supergroup, South Africa). *Precamb.*
813 *Res.* **169**, 1-14.
- 814 Knoll, A.H., and Swett, K. (1990) Carbonate Deposition during the Late Proterozoic Era
815 - an Example from Spitsbergen. *American Journal of Science* **290A**, 104-132.
- 816 Knoll, A.H., Swett, K., and Burkhardt, E. (1989) Paleoenvironmental Distribution of
817 Microfossils and Stromatolites in the Upper Proterozoic Backlundtoppen
818 Formation, Spitsbergen. *Journal of Paleontology* **63**, 129-145.
- 819 Knoll, A.H., Swett, K., and Mark, J. (1991) Paleobiology of a Neoproterozoic Tidal Flat
820 Lagoonal Complex - the Draken Conglomerate Formation, Spitsbergen. *Journal*
821 *of Paleontology* **65**, 531-570.
- 822 Macdonald, F.A., Cohen, P.A., Dudas, F.O., and Schrag, D.P. (2010) Early
823 Neoproterozoic scale microfossils in the Lower Tindir Group of Alaska and the
824 Yukon Territory. *Geology* **38**, 143-146.
- 825 Macdonald, F.A., Smith, E. F., Strauss, J. V., Cox, G. M., Halverson, G. P. & Roots, C.
826 F. (2011). Neoproterozoic and early Paleozoic correlations in the western Ogilvie

827 Mountains, Yukon. In: MacFarlane, K. E., Weston, L. H. & Blackburn, L. R.
828 (eds) *Yukon Exploration and Geology 2010*. Yukon Geological Survey,
829 Whitehorse, 161–182.

830 Maliva, R.G., Knoll, A.H., and Siever, R. (1989) Secular change in chert distribution: a
831 reflection of evolving biological participation in the silica cycle. *Palaios* **4**, 519-
832 532.

833 Maliva, R.G., Knoll, A.H., and Simonson, B.M. (2005) Secular change in the
834 Precambrian silica cycle: Insights from chert petrology. *Geological Society of*
835 *America Bulletin* **117**, 835-845.

836 Marin, J., Chaussidon, M., and Robert, F. (2010) Microscale oxygen isotope variations in
837 1.9 Ga Gunflint cherts: Assessments of diagenesis effects and implications for
838 oceanic paleotemperature reconstructions. *Geochim. Cosmochim. Acta* **74**, 116-
839 130.

840 Marin-Carbonne, J., Chaussidon, M., Boiron, Marie-Christine and Robert, F. (2011) A
841 combined in situ oxygen, silicon isotopic and fluid inclusion study of a chert
842 sample from Onverwacht Group (3.35 Ga, South Africa): New constraints on
843 fluid circulation. *Chem. Geol.* **286**, 59-71.

844 Meheut, M., Lazzeri, M., Balan, E., and Mauri, F. (2007) Equilibrium isotopic
845 fractionation in the kaolinite, quartz, water system: Prediction from first-
846 principles density-functional theory. *Geochim. Cosmochim. Acta* **71**, 3170-3181.

847 Opfergelt, S., Cardinal, D., Andre, L., Delvigne, C., Bremond, L., and Delvaux, B. (2010)
848 Variations of $\delta^{30}\text{Si}$ and Ge/Si with weathering and biogenic input in tropical
849 basaltic ash soils under monoculture. *Geochim. Cosmochim. Acta* **74**, 225-240.

850 Opfergelt, S., de Bournonville, G., Cardinal, D., Andre, L., Delstanche, S., and Delvaux,
851 B. (2009) Impact of soil weathering degree on silicon isotopic fractionation
852 during adsorption onto iron oxides in basaltic ash soils, Cameroon. *Geochim.*
853 *Cosmochim. Acta* **73**, 7226-7240.

854 Piegras, D.J., and Jacobsen, S.B. (1988) The Isotopic Composition of Neodymium in
855 the North Pacific. *Geochim. Cosmochim. Acta* **52**, 1373-1381.

856 Piepgras, D.J., and Jacobsen, S.B. (1992) The Behavior of Rare-Earth Elements in
857 Seawater - Precise Determination of Variations in the North Pacific Water
858 Column. *Geochim. Cosmochim. Acta* **56**, 1851-1862.

859 Pisarevsky S.A., Wingate M.T.D., Powell C. McA., Johnson S. & Evans D.A.D. (2003)
860 Models of Rodinia assembly and fragmentation. In *Proterozoic East Gondwana:
861 Super Continent Assembly and Break-up* (eds. M. Yoshida, B. Windley & S.
862 Dasgupta), Geological Society of London Special Publication, 206, pp 35-55.

863 Planavsky, N.J., McGoldrick, P., Scott, C.T., Li, C., Reinhard, C.T., Kelly, A.E., Chu, X.,
864 Bekker, A., Love, G.D., and Lyons, T.W. (2011) Widespread iron-rich
865 conditions in the mid-Proterozoic ocean. *Nature*, doi:10.1038/nature10327.

866 Pokrovsky, O.S., Pokrovski, G.S., Schott, J., and Galy, A. (2006) Experimental study of
867 germanium adsorption on goethite and germanium co-precipitation with iron
868 hydroxide: X-ray absorption fine structure and macroscopic characterization.
869 *Geochim. Cosmochim. Acta* **70**, 3325-3341.

870 Pope, E.C., Bird, D.K., and Rosing, M.T. (2012) Isotope composition and volume of
871 Earth's early oceans. *Proc. Nat. Acad. Sci, USA* **109**, 4371-4376.

872 Posth, N.R., Hegler, F., Konhauser, K.O., and Kappler, A. (2008) Alternating Si and Fe
873 deposition caused by temperature fluctuations in Precambrian oceans. *Nature
874 Geoscience* **1**, 703-708.

875 Reynolds, B.C., Aggarwal, J., Andre, L., Baxter, D., Beucher, C., Brzezinski, M.A.,
876 Engstrom, E., Georg, R.B., Land, M., Leng, M.J., Opfergelt, S., Rodushkin, I.,
877 Sloane, H.J., van den Boorn, S.H.J.M., Vroon, P.Z., and Cardinal, D. (2007) An
878 inter-laboratory comparison of Si isotope reference materials. *J. Anal. Atom.
879 Spectrom.* **22**, 561-568.

880 Reynolds, B.C., Jaccard, S.L., and Haliday, A.N. (2006) Abrupt cessation of north pacific
881 upwelling with Northern Hemisphere Glaciation recorded by silicon isotopes.
882 *Geochim. Cosmochim. Acta* **70**, A530 (Abstr.).

883 Robert, F., and Chaussidon, M. (2006) A palaeotemperature curve for the Precambrian
884 oceans based on silicon isotopes in cherts. *Nature* **443**, 969-972.

885 Savage, P.S., Georg, R.B., Armytage, R.M.G., Williams, H.M., and Halliday, A.N.
886 (2010) Silicon isotope homogeneity in the mantle. *Earth Planet. Sci. Lett.* **295**,
887 139-146.

888 Sergeev, V.N., Knoll, A.H., and Grotzinger, J.P. (1995) Paleobiology of the
889 Mesoproterozoic Billyakh Group, Anabar uplift, Northern Siberia. *Paleontological*
890 *Society Mem.* **39**, 1-37.

891 Sergeev, V.N., Knoll, A.H., and Petrov, P.Yu. (1997) Paleobiology of the late
892 Mesoproterozoic Sukhaya Tunguska Formation, Turukhansk Uplift, northeastern
893 Siberia. *Precamb. Res.* **85**, 201-239.

894 Shields, G., and Veizer, J. (2002) Precambrian marine carbonate isotope database:
895 Version 1.1. *Geochemistry Geophysics Geosystems* **3**, 10.1029/2001GC000266.

896 Siever, R. (1991) Silica in the oceans: Biological-geochemical interplay, in *Scientists on*
897 *Gaia* (eds. S. Schneider and P. J. Boston), MIT press, pp. 287-295.

898 Siever, R. (1992) The Silica Cycle in the Precambrian. *Geochim. Cosmochim. Acta* **56**,
899 3265-3272.

900 Steinhoefel, G., Horn, I., and von Blanckenburg, F. (2009) Micro-scale tracing of Fe and
901 Si isotope signatures in banded iron formation using femtosecond laser ablation.
902 *Geochim. Cosmochim. Acta* **73**, 5343-5360.

903 Steinhoefel, G., von Blanckenburg, F., Horn, I., Konhauser, K.O., Beukes, N.J., and
904 Gutzmer, J. (2010) Deciphering formation processes of banded iron formations
905 from the Transvaal and the Hamersley successions by combined Si and Fe isotope
906 analysis using UV femtosecond laser ablation. *Geochim. Cosmochim. Acta* **74**,
907 2677-2696.

908 Strother, P.K., Knoll, A.H., and Barghoorn, E.S. (1983) Microorganisms from the Late
909 Precambrian Narssarssuk Formation, Northwestern Greenland. *Palaeontology* **26**,
910 1-32.

911 Tobin, K.J. (1990) The Paleocology and Significance of the Gunflint-Type Microbial
912 Assemblages from the Frere Formation (Early Proterozoic), Nabberu Basin,
913 Western-Australia. *Precamb. Res.* **47**, 71-81.

914 Tosca, N.J., Johnston, D.T., Mushegian, A., Rothman, D.H., and Knoll, A.H. (2010) Clay
915 mineralogy, organic carbon burial, and redox evolution in Proterozoic oceans.
916 *Geochim. Cosmochim. Acta* **74**, 1579-1592.

917 Treguer, P., Nelson, D.M., Vanbennekom, A.J., Demaster, D.J., Leynaert, A., and
918 Queguiner, B. (1995) The Silica Balance in the World Ocean - a Reestimate.
919 *Science* **268**, 375-379.

920 van den Boorn, S.H.J.M., van Bergen, M.J., Nijman, W., and Vroon, P.Z. (2007) Dual
921 role of seawater and hydrothermal fluids in Early Archean chert formation:
922 Evidence from silicon isotopes. *Geology* **35**, 939-942.

923 van den Boorn, S.H.J.M., van Bergen, M.J., Vroon, P.Z., de Vries, S.T., and Nijman, W.
924 (2010) Silicon isotope and trace element constraints on the origin of ~3.5 Ga
925 cherts: Implications for Earth Archaean marine environments. *Geochim.*
926 *Cosmochim. Acta* **74**, 1077-1103.

927 van den Boorn, S.H.J.M., Vroon, P.Z., van Belle, C.C., van der Wagt, B., Schwieters, J.,
928 and van Bergen, M.J. (2006) Determination of silicon isotope ratios in silicate
929 materials by high-resolution MC-ICP-MS using a sodium hydroxide sample
930 digestion method. *J. Anal. Atom. Spectrom.* **21**, 734-742.

931 Varela, D. E., Pride, C. J., and Brzezinski, M. A. (2004) Biological fractionation of
932 silicon isotopes in Southern Ocean surface waters. *Global Biogeochem. Cycles*
933 **18**, GB1047, doi:10.1029/2003GB002140.

934 Walter, M.R., Goode, A.D.T., and Hall, W.D.M. (1976) Microfossils from a newly
935 discovered Precambrian stromatolitic iron formation in Western Australia. *Nature*
936 **261**, 221-223.

937 Weyer, S., and Schwieters, J. (2003) High precision Fe isotope measurements with high
938 mass resolution MC-ICPMS. *Int. J. Mass. Spectrom.* **226**, 355-368.

939 Wilson, J.P., Fischer, W.W., Johnston, D.T., Knoll, A.H., Grotzinger, J.P., Walter, M.R.,
940 McNaughton, N.J., Simon, M., Abelson, J., Schrag, D.P., Summons, R., Allwood,
941 A., Andres, M., Gammon, C., Garvin, J., Rashby, S., Schweizer, M., and Watters,
942 W.A. (2010) Geobiology of the late Paleoproterozoic Duck Creek Formation,
943 Western Australia. *Precam. Res.* **179**, 135-149. Ziegler, K., Chadwick, O.A.,
944 Brzezinski, M.A., and Kelly, E.F. (2005) Natural variations of delta Si-30 ratios

945 during progressive basalt weathering, Hawaiian Islands. *Geochim. Cosmochim.*
946 *Acta* **69**, 4597-4610.

947 Li Yi-Liang, L., Konhauser, K. O., Cole, D. R. et al. (2011) Mineral ecophysiological
948 data provide growing evidence for microbial activity in banded-iron formations.
949 *Geology* **39**, 707-710 DOI: 10.1130/G32003.1.

950 Ziegler, K., Marin-Carbonne, J., McKeegan, K. D., and Young, E. D. (2011) Silicon and
951 oxygen isotope values of cherts and their precursors. *Mineralogical Magazine*
952 **75(3)**, 2284.

953

954

955 **FIGURE CAPTIONS**

956

957 **Figure 1.** Illustrative examples of cherts measured in this study, showing petrography
958 and retention of micron scale features within cherts. Silicification occurred early in
959 diagenesis, and the samples show little evidence for later diagenetic modification. A.
960 Thin section of silicified lagoonal carbonate from the Akademikerbreen Group, Svalbard:
961 silicified clasts, largely of microbial mats, are light brown; grey clasts and cements are
962 dolomite; B and C, cyanobacterial microfossils preserved in early diagenetic chert
963 samples from the Akademikerbreen Group (B) and the Bil'yakh Group, Siberia. D.
964 Bil'yakh chert showing preservation of depositional texture, most conspicuously, sub-mm
965 scale aragonite crystals. Scale bar in C = 4 mm for A, = 20 microns for B, = 40 microns
966 for C, and = 1 mm for D.

967

968 **Figure 2. (a)** Si isotopic composition of the cherts samples analyzed in this study as a
969 function of their depositional age estimates. Open and filled blue symbols are peritidal
970 cherts while blue crosses and pluses are cherts which formed by replacements of basinal
971 carbonates. Red symbols are banded iron formations (BIF).

972 **(b)** All available bulk rock and in-situ MC-ICPMS data as well as in-situ ion-probe and
973 SIMS results for cherts including our data (blue and red crosses). Data for Archean cherts
974 are from Isua (BIFs, Andre et al., 2006), C and S cherts (van den Boorn et al., 2007,
975 2010), Onverwacht Group cherts (Abraham et al., 2011), Old Wanderer Formation BIFs

976 (Steinboefel et al., 2009) and the Dales Gorge, Kuruman and Penge BIFs (Steinboefel et
977 al., 2010). Error bars for all MC-ICPMS and SIMS data are smaller than the size of the
978 symbols. Ion probe data of Robert and Chaussidon (2006) are plotted with 2σ error bars
979 after correcting the ages of some of their samples based on more updated age estimates.
980 The ages have been corrected for samples from the Dengying Fm. (550Ma), Tindir Creek
981 (717-811 Ma), Pahrump Group (720-800 Ma), Amadeus Basin (800 Ma), Jixian Group
982 (1400-1600 Ma), McAurthur Basin (1590-1650 Ma), Nabberu Basin (1800 Ma), Wyllö
983 Group (1800-1900 Ma), Gunflint Fm. (1850-1900 Ma), Transvaal Basin (2500-2600 Ma),
984 Rietgat Fm. (2700 Ma), Keewatin Fm. (2700 Ma), and Manjeri Fm. (2700 Ma). The ion-
985 probe data of Robert and Chaussidon (2006) show a broadly similar temporal trend as the
986 MC-ICPMS data.

987

988 **Figure 3. (a)** A histogram of $\delta^{30}\text{Si}$ of cherts analyzed in this study plotted against the
989 frequency of samples. Red indicates basinal cherts associated with BIFs whereas blue
990 indicates non-BIF cherts.

991 **(b)** A compilation of all MC-ICPMS Si isotope data for Precambrian cherts including our
992 data. Literature data are from Isua (BIFs, Andre et al., 2006), Pilbara craton (C and S
993 cherts, van den Boorn et al., 2007, 2010), Onverwacht Group cherts (Abraham et al.,
994 2011), Old Wanderer Formation BIFs (Steinboefel et al., 2009) and the Dales Gorge,
995 Kuruman and Penge BIFs (Steinboefel et al., 2010). It is clear that BIFs typically show
996 lower $\delta^{30}\text{Si}$ compared to non-BIF cherts that were deposited in peritidal environments.

997

998 **Figure 4.** A simple isotope fractionation model showing open system (Rayleigh
999 fractionation) and closed system (equilibrium fractionation) variation of $\delta^{30}\text{Si}$ as a
1000 function of silica left in the residual solution (f). In the present context, the solution is
1001 silica saturated porewater (PW) while the precipitating solid are cherts. The $\delta^{30}\text{Si}$ of the
1002 initial porewater is taken as 0.8. In case 1, the Si isotope fractionation factor between PW
1003 (long-dashed lines) and cherts (solid lines) is assumed to be -2.0 ‰ and in case 2, it is
1004 taken as -3.0 ‰ (see text for details). Large $\delta^{30}\text{Si}$ variations in cherts from a single basin,
1005 as observed in the Spitsbergen cherts of the present study (~ 3.0 ‰), can be explained by
1006 Rayleigh-type fractionation with f ranging from 1 to 0.2 (grey and black arrows).

1007 Fractionations are much smaller for the equilibrium/closed-system scenario and require
1008 much lower values of f .

Table 1.

Sample #	Age (Ma)	Location	$\delta^{29}\text{Si}$	2SE	$\delta^{30}\text{Si}$	2SE	N	Other information (reference)
86P-121	750	Akademikerbreen Gr., Spitsbergen, Svalbard, Norway	-0.26	0.05	-0.51	0.06	3	Peritidal, silicified carbonate (1)
81P-4918	750	Akademikerbreen Gr., Spitsbergen, Svalbard, Norway	-0.90	0.03	-1.78	0.04	7	Peritidal, silicified carbonate (1)
81P-4705-2B	750	Akademikerbreen Gr., Spitsbergen, Svalbard, Norway	0.52	0.03	1.04	0.05	6	Peritidal, silicified carbonate (1)
86M-20-3	750	Akademikerbreen Gr., Spitsbergen, Svalbard, Norway	0.34	0.04	0.67	0.08	7	Peritidal, silicified carbonate (1)
81B-670	750	Akademikerbreen Gr., Spitsbergen, Svalbard, Norway	0.07	0.03	0.15	0.08	8	Peritidal, silicified carbonate (1)
81B-625-2A	750	Akademikerbreen Gr., Spitsbergen, Svalbard, Norway	-0.31	0.04	-0.62	0.07	7	Peritidal, silicified carbonate (1)
81B-550	750	Akademikerbreen Gr., Spitsbergen, Svalbard, Norway	-0.08	0.02	-0.14	0.06	9	Peritidal, silicified carbonate (1)
86P-96-2A	750	Akademikerbreen Gr., Spitsbergen, Svalbard, Norway	0.12	0.06	0.25	0.08	7	Peritidal, silicified carbonate (1)
86P-96	750	Akademikerbreen Gr., Spitsbergen, Svalbard, Norway	-0.22	0.05	-0.43	0.07	8	Peritidal, silicified carbonate (1)
86G-54-1	750	Akademikerbreen Gr., Spitsbergen, Svalbard, Norway	0.06	0.03	0.11	0.06	7	Peritidal, silicified carbonate (1)
81P-4353	750	Akademikerbreen Gr., Spitsbergen, Svalbard, Norway	-0.25	0.01	-0.48	0.03	6	Peritidal, silicified carbonate (1)
81P-4350-2	750	Akademikerbreen Gr., Spitsbergen, Svalbard, Norway	0.64	0.02	1.26	0.03	7	Peritidal, silicified carbonate (1)
86P-11-1	750	Akademikerbreen Gr., Spitsbergen, Svalbard, Norway	-0.35	0.04	-0.71	0.08	6	Peritidal, silicified carbonate (1)
86P-11-2	750	Akademikerbreen Gr., Spitsbergen, Svalbard, Norway	0.31	0.06	0.60	0.10	5	Peritidal, silicified carbonate (1)
81B-222	750	Akademikerbreen Gr., Spitsbergen, Svalbard, Norway	0.07	0.05	0.16	0.10	7	Peritidal, silicified carbonate (1)
86P-108-3	750	Akademikerbreen Gr., Spitsbergen, Svalbard, Norway	0.14	0.05	0.29	0.08	3	Peritidal, silicified carbonate (1)
81B-105-1A3	750	Akademikerbreen Gr., Spitsbergen, Svalbard, Norway	-0.69	0.04	-1.38	0.09	6	Peritidal, silicified carbonate (1)
SV-6	750	Akademikerbreen Gr., Spitsbergen, Svalbard, Norway	-0.01	0.05	-0.03	0.06	7	Peritidal, silicified carbonate (1)
SV-4	750	Akademikerbreen Gr., Spitsbergen, Svalbard, Norway	0.18	0.04	0.35	0.09	4	Peritidal, silicified carbonate (1)
81P-3400-3A	750	Akademikerbreen Gr., Spitsbergen, Svalbard, Norway	-0.30	0.02	-0.62	0.04	9	Peritidal, silicified carbonate (1)
81P-4077	750	Akademikerbreen Gr., Spitsbergen, Svalbard, Norway	-0.56	0.02	-1.14	0.05	7	Peritidal, silicified carbonate (1)
81P-5570	750	Akademikerbreen Gr., Spitsbergen, Svalbard, Norway	-0.33	0.05	-0.64	0.07	6	Peritidal, silicified carbonate (1)
T-714-1	770	Fifteenmile Gr., Alaska	-0.52	0.05	-1.03	0.06	8	Shallow subtidal, silicified carbonate (2)
T-714-2	770	Fifteenmile Gr., Alaska	-0.26	0.02	-0.51	0.03	7	Shallow subtidal, silicified carbonate (2)
E19-6-1	800	Limestone-Dolomite Series, east Greenland	-0.32	0.04	-0.61	0.08	8	Peritidal, silicified carbonate (3)
GR15-5	800	Limestone-Dolomite Series, east Greenland	-0.16	0.04	-0.32	0.07	8	Peritidal, silicified carbonate (3)
K1272	800	Hunnberg Fm., Nordaustlandet, Svalbard, Norway	0.00	0.04	-0.02	0.06	9	Peritidal, silicified carbonate (4)
K95-93	1000-1100	Sukhaya Tunguska Fm., NW Siberia	0.18	0.05	0.34	0.09	6	Peritidal, silicified carbonate (5)
K95-94	1000-1101	Sukhaya Tunguska Fm., NW Siberia	0.15	0.04	0.29	0.08	7	Peritidal, silicified carbonate (5)
K95-97	1000-1102	Sukhaya Tunguska Fm., NW Siberia	0.21	0.03	0.41	0.04	7	Peritidal, silicified carbonate (5)
K95-99	1000-1103	Sukhaya Tunguska Fm., NW Siberia	0.63	0.03	1.24	0.06	6	Peritidal, silicified carbonate (5)
K95-102	1000-1104	Sukhaya Tunguska Fm., NW Siberia	1.02	0.03	2.02	0.04	7	Peritidal, silicified carbonate (5)

Sample #	Age (Ma)	Location	$\delta^{29}\text{Si}$	2SE	$\delta^{30}\text{Si}$	2SE	N	Other information (reference)
KS78-21	1200	Narssarssuk Fm., NW Greenland	0.59	0.03	1.19	0.06	8	Peritidal, silicified carbonate (6)
KS78-1	1200	Narssarssuk Fm., NW Greenland	0.48	0.03	0.95	0.06	7	Peritidal, silicified carbonate (6)
KS78-2	1200	Narssarssuk Fm., NW Greenland	0.39	0.04	0.77	0.09	6	Peritidal, silicified carbonate (6)
KS78-5	1200	Narssarssuk Fm., NW Greenland	0.38	0.05	0.76	0.10	6	Peritidal, silicified carbonate (6)
KS78-12	1200	Narssarssuk Fm., NW Greenland	-0.31	0.06	-0.61	0.09	7	Peritidal, silicified carbonate (6)
KS78-14	1200	Narssarssuk Fm., NW Greenland	0.17	0.02	0.33	0.04	7	Peritidal, silicified carbonate (6)
KS78-15	1200	Narssarssuk Fm., NW Greenland	0.74	0.02	1.46	0.06	6	Peritidal, silicified carbonate (6)
KS78-18	1200	Narssarssuk Fm., NW Greenland	0.34	0.04	0.67	0.07	6	Peritidal, silicified carbonate (6)
A2-37855	1200	Society Cliffs Fm., Baffin Island, Canada	0.03	0.04	0.05	0.05	10	Peritidal, silicified carbonate (7)
WE 1740	1200	Society Cliffs Fm., Baffin Island, Canada	0.42	0.04	0.85	0.06	8	Peritidal, silicified carbonate (7)
KG-92-70	1450-1500	Yusmastakh Fm., Billyakh Gr., Siberia	0.91	0.03	1.81	0.04	12	Peritidal, silicified carbonate (8)
KG92-64-4A	1450-1500	Yusmastakh Fm., Billyakh Gr., Siberia	0.90	0.03	1.79	0.06	7	Peritidal, silicified carbonate (8)
KG92-60-2	1450-1500	Yusmastakh Fm., Billyakh Gr., Siberia	0.92	0.03	1.82	0.04	5	Peritidal, silicified carbonate (8)
KG92-57	1450-1500	Yusmastakh Fm., Billyakh Gr., Siberia	0.33	0.04	0.65	0.07	4	Peritidal, silicified carbonate (8)
KG92-59	1450-1500	Yusmastakh Fm., Billyakh Gr., Siberia	1.43	0.05	2.85	0.08	6	Peritidal, silicified carbonate (8)
KG92-61	1450-1500	Yusmastakh Fm., Billyakh Gr., Siberia	0.75	0.04	1.49	0.06	8	Peritidal, silicified carbonate (8)
KG92-67	1450-1500	Yusmastakh Fm., Billyakh Gr., Siberia	1.27	0.04	2.53	0.07	4	Peritidal, silicified carbonate (8)
KG92-30	1450-1500	Kotuikan Fm., Billyakh Gr., Siberia	0.06	0.03	0.11	0.05	9	Peritidal, silicified carbonate (8)
KG92-34	1450-1500	Kotuikan Fm., Billyakh Gr., Siberia	0.11	0.03	0.22	0.06	9	Peritidal, silicified carbonate (8)
KG92-40	1450-1500	Kotuikan Fm., Billyakh Gr., Siberia	-0.11	0.02	-0.20	0.04	7	Peritidal, silicified carbonate (8)
KG92-47	1450-1500	Kotuikan Fm., Billyakh Gr., Siberia	0.07	0.03	0.13	0.05	7	Peritidal, silicified carbonate (8)
F-1	1800	Frere Fm., W Australia	-1.35	0.08	-2.68	0.15	6	Oolitic IF (9)
DCC37	1880	Duck Creek Fm., W Australia	-0.94	0.02	-1.86	0.05	9	Basinal, associated with IF (10)
DCC10	1880	Duck Creek Fm., W Australia	-2.15	0.05	-4.29	0.07	6	Basinal, associated with IF (10)
DC08	1880	Duck Creek Fm., W Australia	-0.79	0.03	-1.57	0.06	7	Basinal, associated with IF (10)
DC38	1880	Duck Creek Fm., W Australia	-0.95	0.03	-1.91	0.05	7	Basinal, associated with IF (10)
GF70-32	1880	Gunflint Fm., Canada	-0.49	0.02	-1.01	0.04	10	Stromatolitic IF (11)
GF66-3a	1880	Gunflint Fm., Canada	-0.42	0.05	-0.82	0.09	6	Basinalchert, with siderite (11)
B-1	1880	Biwabik Fm., Minnesota, USA	-0.71	0.06	-1.42	0.10	7	Hematiticstromatolitic IF (12)

Sample #	Age (Ma)	Location	$\delta^{29}\text{Si}$	2SE	$\delta^{30}\text{Si}$	2SE	N	Other information (reference)
A68-10	2500	Brockman Fm., Hamersley Gr. Australia	-0.31	0.05	-0.61	0.08	6	Banded IF (13)
A68-2	2570	Wittenoom Fm., Hamersley Gr. Australia	-0.55	0.03	-1.11	0.04	8	Chert in basinal dolomite (13)
P7	2530	Griqualand West, Transvaal SG., S Africa	0.17	0.05	0.33	0.10	5	Basinal, BIF (14)
P21	2530	Griqualand West, Transvaal SG., S Africa	0.26	0.05	0.51	0.11	4	Basinal, BIF (14)
GKF 896.14	2530	Griqualand West, Transvaal SG., S Africa	-0.55	0.03	-1.11	0.06	6	Basinal, BIF (14)
GKF 896.34	2530	Griqualand West, Transvaal SG., S Africa	0.29	0.05	0.57	0.08	8	Basinal, BIF (14)
GKF 896.47	2530	Griqualand West, Transvaal SG., S Africa	0.15	0.03	0.28	0.05	4	Basinal, BIF (14)
GKF 897.26	2530	Griqualand West, Transvaal SG., S Africa	-0.35	0.03	-0.71	0.06	9	Basinal, BIF (14)
Ga13	2530	Griqualand West, Transvaal SG., S Africa	0.14	0.02	0.26	0.05	6	Basinal, shale and calcite (14)
Ga17	2530	Griqualand West, Transvaal SG., S Africa	-0.16	0.03	-0.31	0.06	7	Basinal, shale and calcite (14)
Whr 30.1	2530	Griqualand West, Transvaal SG., S Africa	0.71	0.04	1.41	0.08	7	Basinal, shale and calcite (14)
MonT. 450m	2530	Griqualand West, Transvaal SG., S Africa	0.09	0.05	0.20	0.08	6	Peritidal dolomite (14)
Kg10	2530	Griqualand West, Transvaal SG., S Africa	0.91	0.02	1.81	0.04	7	Peritidal dolomite (14)
Kg20	2530	Griqualand West, Transvaal SG., S Africa	0.74	0.04	1.48	0.08	5	Peritidal dolomite (14)

Table 1. Stable Si isotope data for 2570-750 Ma old cherts analyzed in this study from different geographic locations. The uncertainty for $\delta^{29}\text{Si}$ and $\delta^{30}\text{Si}$ measurements are given as $2\sigma_m$ and N denotes the number of repeat measurements. Also shown are available information on the depositional facies and precursor rock type. References describing detailed sedimentology and petrography of these samples are as follows: 1. Knoll et al. 1989,1991; 2. Allison and Awramik, 1989; Macdonald et al., 2010, 2011; 3. Green et al., 1989; 4. Knoll, 1984; 5. Sergeev et al. 1997; 6. Strother et al., 1983; 7. Kah and Knoll, 1996; 8. Sergeev et al., 1995; 9. Walter et al., 1976, Tobin, 1990; 10. Wilson et al., 2010; 11. Barghoorn and Tyler 1965; 12. Brotton et al., 2007; 13. Yi-Liang et al., 2011; 14. Knoll and Beukes, 2009, Fischer and Knoll, 2009.

Table 2. A compilation of estimated Si concentrations and fluxes to the modern and Precambrian oceans as well as the isotopic compositions ($\delta^{30}\text{Si}$) of modern seawater, igneous rocks, and hydrothermal and continental fluxes of Si to the modern ocean. Also listed are the isotopic fractionation factors ($\Delta^{30}\text{Si}$) between seawater and diatoms¹, seawater and sponges², diatoms and fluids (after diatom dissolution)³, Si rich fluid and silica adsorbed on to Fe hydroxides⁴, and quartz and kaolinite⁵. Note that both biologically and physically precipitated silica preferentially incorporates lighter Si isotopes. See text for details.

	Modern Ocean	Precambrian Ocean
Average Si concentration	2 ppm (<1 ppm to 15 ppm)	120-140 ppm
Continental influx of Si	5.5 ± 1.2 Tmoles/year	
Marine/Hydrothermal influx of Si	0.6 ± 0.3 Tmoles/year	
Biological outflux of Si	7.1 ± 1.8 Tmoles/year	
Residence time of Si	~15,000 years	0.9 - 1.05 Ma
Average $\delta^{30}\text{Si}$ (modern seawater)	1.1	
$\delta^{30}\text{Si}$ (igneous rocks)	-0.39	
$\delta^{30}\text{Si}$ (hydrothermal flux to modern sw)	-0.4	
$\delta^{30}\text{Si}$ (continental flux to modern sw)	0.8	
$\Delta^{30}\text{Si}$ (seawater - diatoms) ¹	1.1	
$\Delta^{30}\text{Si}$ (seawater - sponges) ²	3.5	
$\Delta^{30}\text{Si}$ (diatoms - fluid) ³	0.55	
$\Delta^{30}\text{Si}$ (fluid - silica adsorbed onto Fe hydroxides) ⁴	1.1 to 1.6	
$\Delta^{30}\text{Si}$ (quartz - kaolinite) ⁵	1.6	

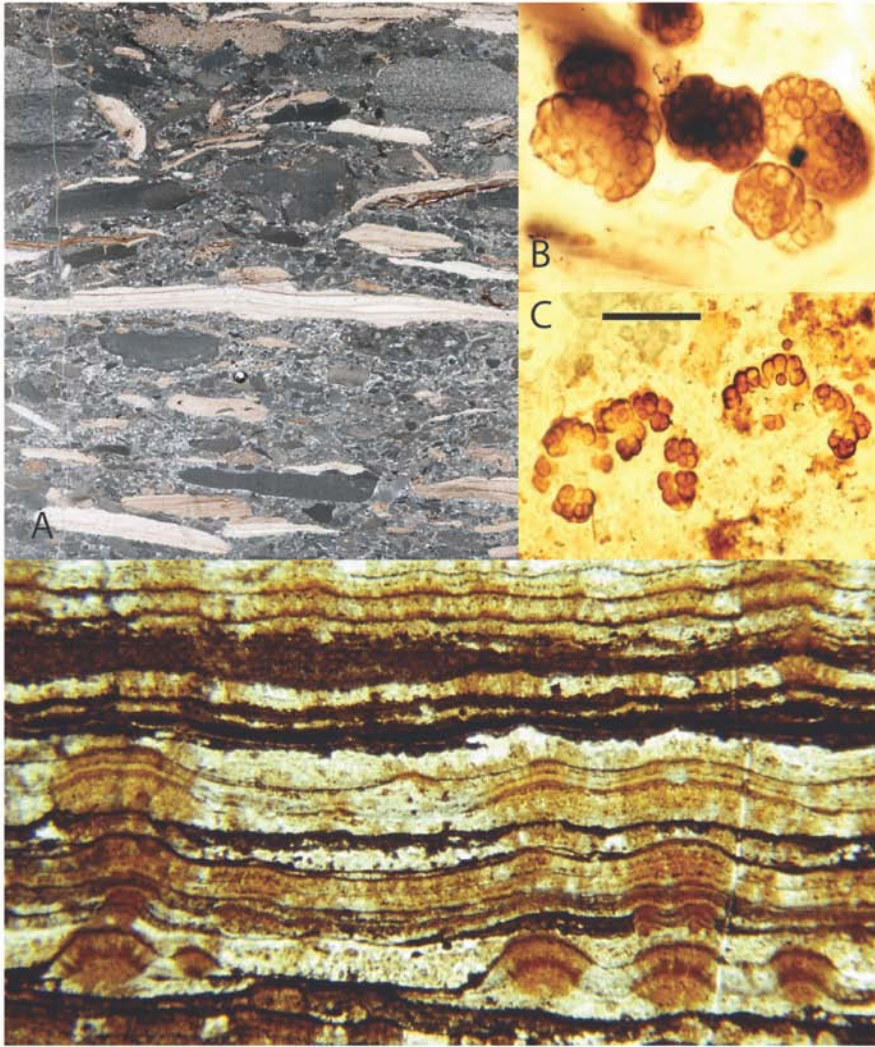


Figure 1.

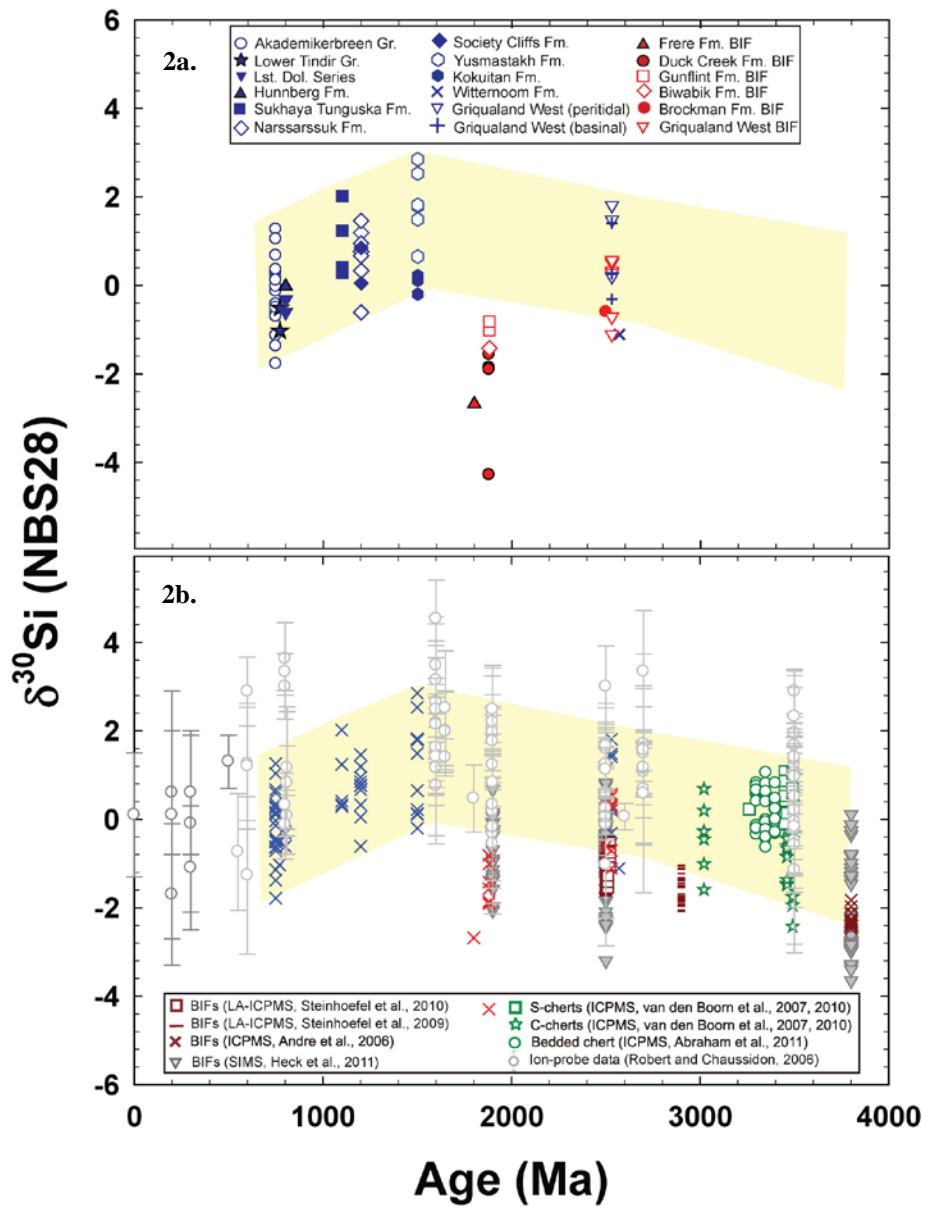


Figure 2.

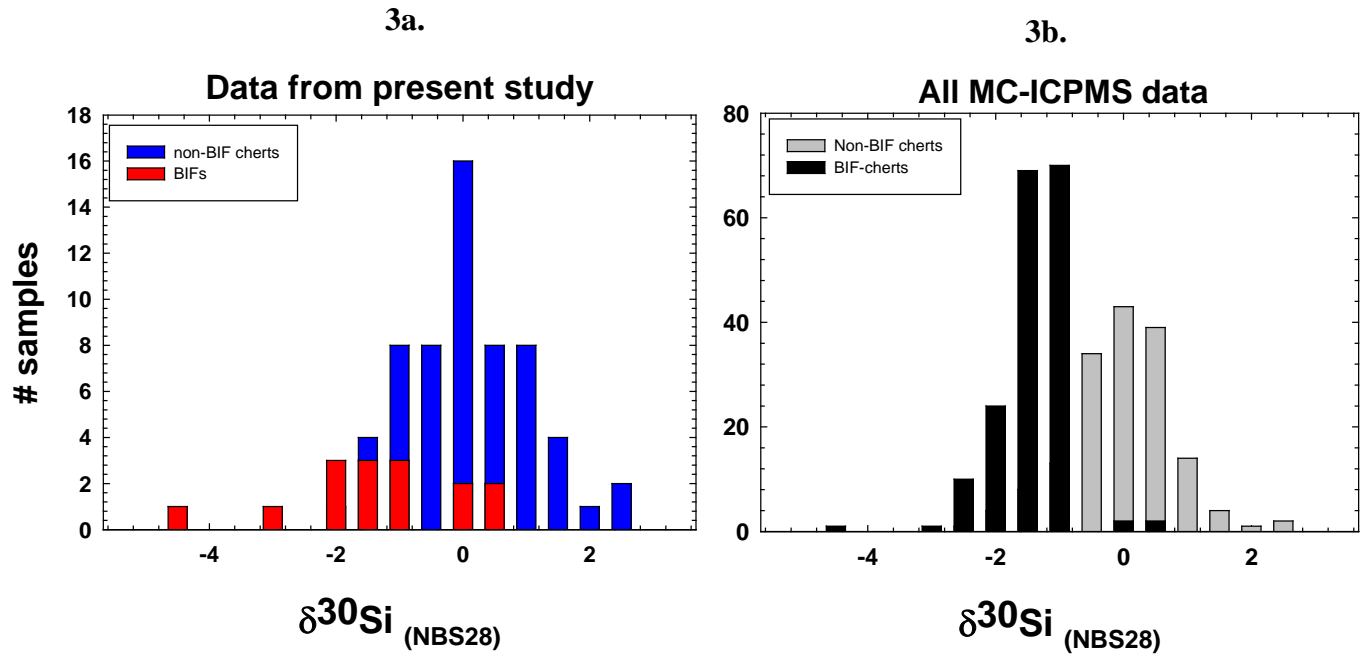


Figure 3.

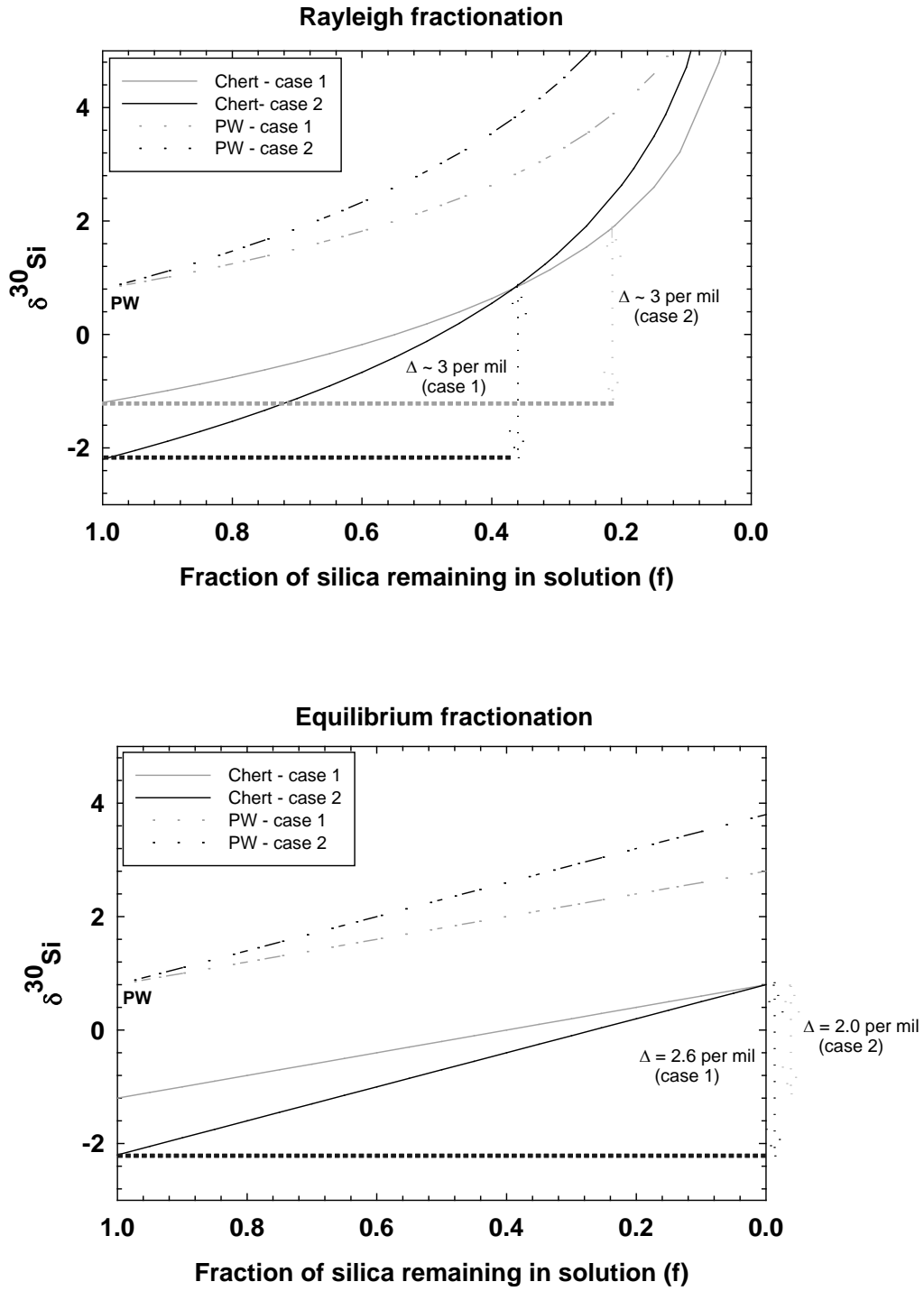


Figure 4.